Empirical Analysis of Performance Bottlenecks in Graph Neural Network Training and Inference with GPUs

Zhaokang Wang, Yunpan Wang, Chunfeng Yuan, Rong Gu* , Yihua Huang*

State Key Laboratory for Novel Software Technology,
Department of Computer Science and Technology, Nanjing University,
Nanjing 210023, China

Abstract

The graph neural network (GNN) has become a popular research area for its state-of-the-art performance in many graph analysis tasks. Recently, various graph neural network libraries have emerged. They make the development of GNNs convenient, but their performance bottlenecks on large datasets are not well studied. In this work, we analyze the performance bottlenecks in GNN training and inference with GPUs empirically. A GNN layer can be decomposed into two parts: the vertex and the edge calculation parts. According to their computational complexity, we select four representative GNNs (GCN, GGNN, GAT, GaAN) for evaluation. We decompose their running time and memory usage, evaluate the effects of hyper-parameters and assess the efficiency of the sampling techniques. The experimental evaluation with PyTorch Geometric indicates that the edge-related calculation is the performance bottleneck for most GNNs, dominating the training/inference time and memory usage. The sampling techniques are essential for GNN training and inference on big graphs with GPUs, but their current implementation still has non-trivial overheads in sampling and data transferring.

Keywords: graph neural network, performance bottleneck analysis, empirical evaluation, machine learning system, GPU

1. Introduction

In recent years, the graph neural network (GNN) becomes a hot research topic in the field of artificial intelligence. Many GNNs [1, 2, 3, 4, 5, 6, 7] are proposed. They can learn the representation of vertices/edges in a graph from its topology and the original feature vectors in an *end-to-end* manner. The powerful expression capability makes GNNs achieve good accuracy in not only graph analytical tasks [8, 9, 10] (like node classification and link prediction) but also computer vision tasks (like human-object interaction [11], human parsing [12], and video object segmentation [13]).

To train GNNs easily, a series of GNN libraries/systems [14, 15, 16, 17, 18] are proposed. PyTorch Geometric (PyG) [14], NeuGraph [16], PGL [18] and Deep Graph Library (DGL) [15] build upon the existing deep learning frameworks (PyG on PyTorch, NeuGraph on TensorFlow, PGL on PaddlePaddle, DGL on multiple backends). They provide users with a high-level programming model (the message-passing framework for PyG/PGL/DGL and the SAGA-NN model for NeuGraph) to describe the structure of a GNN. They take advantage of the common tools provided by the underlying frameworks like the automatic differentiation to simplify the development. They utilize specially optimized CUDA kernels (like kernel fusion [15, 16]) and other implementation techniques (like 2D graph partitioning [16]) to improve the speed of GNN training on GPUs.

However, what is the real performance bottleneck in GNN training and inference is still in doubt. Yan et al. [19] and Zhang et al. [20] experimentally analyze the architectural characteristics of GNN *inference*. They find that the GNN inference is more cache-friendly than the traditional graph analysis tasks (like PageRank) and is suitable for GPUs. They verify the effectiveness of the kernel fusion optimization in reducing the time

of inference. Nevertheless, they only analyze the inference stage, ignoring the effects of the backpropagation during training.

To explore essential performance bottlenecks in both GNN training and inference, we conduct a range of experimental analysis in this work. We focus on the efficiency bottlenecks of GNN training and inference. We model the GNNs with the message-passing framework that decomposes a GNN layer into two parts: the vertex calculation and the edge calculation. According to the time complexity of the two parts, we classify the typical GNNs into four quadrants ({high, low} complexity $\times$ {vertex, edge} calculation). We choose GCN [1], GGNN [4], GAT [6], and GaAN [7] as representative GNNs of the four quadrants.

We implement them with PyG and evaluate their efficiency and accuracy with six real-world datasets on a GPU card. We identify the most time-consuming stage in GNN training and inference by decomposing the training and inference time per epoch from the layer level to the operator level. We also analyze the memory usage during training and inference to discover the main factor that limits the data scalability of GNN training and inference on GPUs. Finally, we evaluate whether or not the sampling techniques affect the performance bottlenecks and accuracy. The key findings and insights are summarized below.

- *The training and inference time and the memory usage of a GNN layer are mainly affected by the dimensions of the input/output hidden vectors.* Fixing other hyper-parameters, the training and inference time and the memory usage of a GNN layer increase linearly with the dimensions.

- *The edge-related calculation is the performance bottleneck for most GNNs.* For GNNs with high edge calculation complexity, most of the training and inference time is spent on conducting the messaging function for every edge. For GNNs with low edge calculation complexity, the collection and aggregation of message vectors of all edges consume most of the training and inference time.

- *The high memory usage of the edge calculation stage is the main factor limiting the data scalability of GNN training and inference.* The edge calculation generates (and caches) many intermediate results. They are an order of magnitude larger than the dataset itself. As GPUs have limited on-chip memory, high memory consumption prevents us from performing training and inference on big graphs.

- *The sampling techniques can significantly reduce the memory usage of training and inference.* The sampling techniques are essential for performing GNN training and inference on big graphs with GPUs. The accuracy of the GNN models trained with the sampling techniques is close to the accuracy of full-batch training. However, the existing implementation of sampling is still inefficient. The time spent on sampling may exceed the time spent on training and inference. Under small batch sizes, the sampled graphs are also small, wasting the computing power of GPUs.

Based on the insights, we provide several potential optimization directions:

- To reduce training and inference time, *optimizations should focus on improving the efficiency of the edge calculation*. One may consider developing optimized operators for the messaging step that is the major source of computing costs in the edge calculation. Fusing operators of the collection step, messaging function and the aggregation step together is another way to reduce the overheads in the edge calculation.

- To reduce memory usage, *optimizations should focus on reducing the intermediate results in the edge calculation*. One may consider adopting the checkpoint mechanism to cache less intermediate results during the forward phase and re-calculate the needed data on the fly during the backpropagation.

- To improve the efficiency of the sampling techniques, *one may consider overlapping the sampling on the CPU side with the training/inference on the GPU side.* Choosing a proper batch size automatically is another potential optimization.

We hope that our analysis can help the developers of the GNN libraries/systems have a better understanding of the characteristics of GNN training/inference and propose more targeted optimizations.

Outline. We briefly survey the typical GNNs in Section 2. We introduce our experimental setting and targets in Section 3. The experimental results are presented and analyzed in Section 4. We summarize the key findings and give out potential optimization directions in Section 5. We introduce the related work in Section 6 and conclude our work in Section 7.

2

2. Review of Graph Neural Networks

In this section, we formally define the graph neural networks and briefly survey typical graph neural networks. We denote a simple *undirected* graph $\mathcal{G}$ as $\mathcal{G} = (\mathcal{V}, \mathcal{E})$, where $\mathcal{V}$ and $\mathcal{E}$ are the vertex set and the edge set of $\mathcal{G}$, respectively. We use v_x $(0 \leq x < |\mathcal{V}|)$ to denote a vertex and $e_{y,x} = (v_y, v_x)$ to denote the edge pointing from v_y to v_x. The adjacency set of v_x is $\mathcal{N}(v_x) = \{v|(v, v_x) \in \mathcal{E}\}$. We denote a *vector* with a bold lower case letter like h and a *matrix* with a bold upper case letter like W. Table 1 summarizes the common symbols used throughout this work. We use blue characters w/W to denote weight vectors/matrices that are model parameters to train in a GNN.

Table 1: Frequently-used symbols

Category	Symbol	Meaning
Graph Structure	$\mathcal{G} = (\mathcal{V}, \mathcal{E})$	The simple undirected input graph with the vertex set $\mathcal{V}$ and the edge set $\mathcal{E}$.
	v_x	The x-th vertex of the input graph.
	$e_{y,x}$	The edge pointing from v_y to v_x of the input graph.
	$\mathcal{N}(v_x)$	The adjacency set of v_x in the input graph.
	$\bar{d}$	The average degree of the input graph.
GNN Definition	L	The number of GNN layers.
	K	The number of heads in a GNN layer.
	ϕ^l	The messaging function of the GNN layer l.
	Σ^l	The aggregation function of the GNN layer l.
	γ^l	The vertex updating function of the GNN layer l.
	$\phi^{l,i} \,/\, \Sigma^{l,i} \,/\, \gamma^{l,i}$	The messaging/aggregation/updating function of the i-th sub-layer of the GNN layer l.
	$W^l, W^{(k)}/b, a$	The matrices/vectors represented by the blue characters are the weight matrices/vectors that need to be learned in the GNN.
Vector	v_x	The feature vector of the vertex v_x.
	$e_{y,x}$	The feature vector of the edge $e_{y,x}$.
	h_x^l	The input hidden vector of the graph neuron corresponding to v_x in the GNN layer l.
	h_x^{l+1}	The output hidden vector of the graph neuron corresponding to v_x in the GNN layer l.
	$m_{y,x}^l$	The message vector of the edge $e_{y,x}$ outputted by ϕ^l of the GNN layer l.
	s_x^l	The aggregated vector of the vertex v_x outputted by Σ^l of the GNN layer l.
	$h_x^{l,i} \,/\, m_{y,x}^{l,i} \,/\, s_x^{l,i}$	The hidden/message/aggregated vector of the vertex v_x outputted by $\gamma^{l,i}/\phi^{l,i}/\Sigma^{l,i}$ of the i-th sub-layer of the GNN layer l.
	d_{in}^l, d_{out}^l	The dimension of the input/output hidden vectors of the GNN layer l.
	$dim(x)$	The dimension of a vector x.

2.1. Structure of Graph Neural Networks

As illustrated in Figure 1, a typical GNN can be decomposed into three parts: an input layer + several GNN layers + a prediction layer.

In the input layer, A GNN receives a graph $\mathcal{G}$ as the input. Every vertex v_x in $\mathcal{G}$ is attached with a feature vector v_x to describe the properties of the vertex. Every edge $e_{y,x}$ of $\mathcal{G}$ may also be attached with a feature vector $e_{y,x}$. The input layer of a GNN receives feature vectors from all vertices and passes the feature vectors to the first GNN layer (i.e. GNN layer 0).

A GNN usually consists of more than one GNN layer. Each GNN layer consists of $|\mathcal{V}|$ graph neurons, where $|\mathcal{V}|$ is the number of vertices in $\mathcal{G}$. Each graph neuron corresponds to a vertex in $\mathcal{G}$. Different GNNs mainly differ in the graph neurons that they use. We elaborate on the details of graph neurons later. GNN layers are *sparsely* connected with the input layer and other GNN layers.

- In the first GNN layer (layer 0), a graph neuron collects feature vectors from the input layer. For the graph neuron corresponding to the vertex v_x, it collects the feature vector v_x and the feature vectors v_y of the vertices v_y that are adjacent to v_x (i.e. $v_y \in \mathcal{N}(v_x)$). The graph neuron aggregates input feature vectors, apply non-linear transformation, and outputs a hidden vector h_x^1 for v_x. Take the demo GNN in Figure 1(a) as an example. Since $\mathcal{N}(v_3) = \{v_1, v_2, v_4, v_5, v_6\}$, the graph neuron of v_3 at the GNN
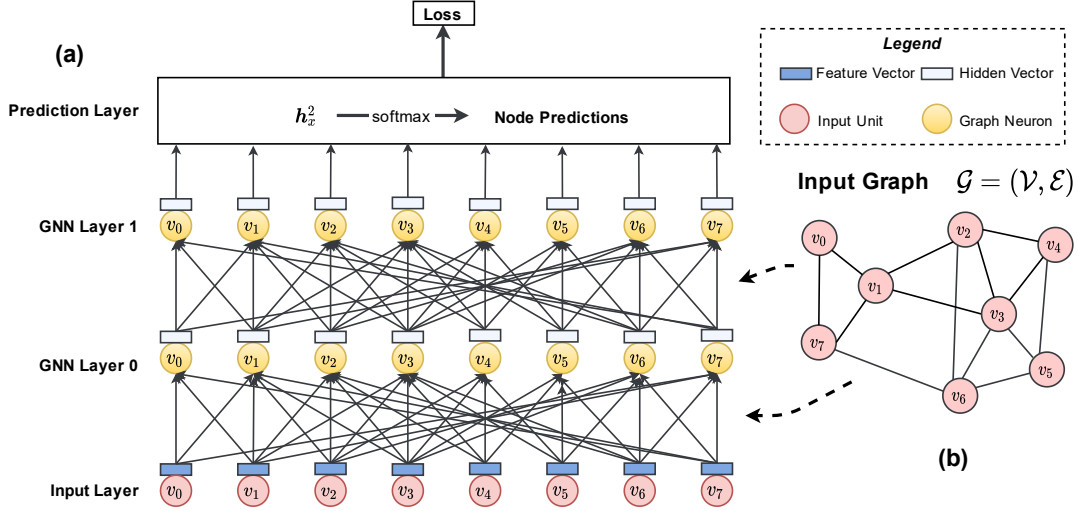
Figure 1: Structure of a typical graph neural network. (a) Demo GNN, (b) Demo graph. The target application is the node classification. The demo GNN has two GNN layers.

layer 0 collects the input feature vectors $\{\boldsymbol{v}_1, \boldsymbol{v}_2, \boldsymbol{v}_3, \boldsymbol{v}_4, \boldsymbol{v}_5, \boldsymbol{v}_6\}$ from the input layer and outputs $\boldsymbol{h}_3^1$. The connections between the first GNN layer and the input layer are determined by the topology of $\mathcal{G}$. The graph neuron of v_x in the first GNN layer is connected with the input unit of v_y in the input layer only if there is an edge $e_{y,x}$ between v_y and v_x in $\mathcal{G}$. Since most real-world graphs are very *sparse* (i.e. $|\mathcal{E}| \ll |\mathcal{V}|^2$), the connections between the first GNN layer and the input layer are also sparse, different from the traditional neural networks.

- In the next GNN layer (layer 1), the graph neuron corresponding to v_x collects the hidden vector of itself $\boldsymbol{h}_x^1$ and its adjacent vertices ($\boldsymbol{h}_y^1$ with $v_y \in \mathcal{N}(v_x)$) from the *previous* GNN layer. Thus, the connections between the first and the second GNN layers are also determined by the topology of $\mathcal{G}$. Based on the collected hidden vectors, the graph neuron in the layer 1 outputs a new hidden vector $\boldsymbol{h}_x^2$ for v_x.

- A GNN allows stacking more GNN layers to support deeper graph analysis. Assume there are L GNN layers in total. The last GNN layer (layer $L-1$) outputs a hidden vector $\boldsymbol{h}_x^L$ for every vertex v_x. $\boldsymbol{h}_x^L$ is an embedding vector that encodes the knowledge learned from the input layer and all the previous GNN layers. Since $\boldsymbol{h}_x^L$ is affected by v_x and the vertices in the L-hop neighborhood of v_x, analyzing a graph with more GNN layers means analyzing each vertex with a *wider* scope. The hidden vectors $\boldsymbol{h}_x^L$ of the last GNN layer are fed to the prediction layer to generate the output for the whole GNN.

The prediction layer is a standard neural network. The structure of the prediction layer depends on the prediction task of the GNN. Take the node classification task in Figure 1 as the example. The node classification predicts a label for every vertex in $\mathcal{G}$. In this case, the prediction layer can be a simple softmax layer with $\boldsymbol{h}_x^L$ as the input and a vector of probabilities as the output. If the prediction task is the edge prediction, the hidden vectors of two vertices are concatenated and fed into a softmax layer. If we need to predict a label for the whole graph, a pooling (max/mean/...) layer is added to generate an embedding vector for the whole graph and the embedding vector is used to produce the final prediction.

Supporting end-to-end training is a prominent advantage of GNNs, compared with traditional graph-based machine learning methods. The traditional methods need to construct input feature vectors for vertices and edges manually or use embedding methods like DeepWalk [21] and node2vec [22]. The feature vector generation is independent of model training. Therefore, generated feature vectors may not be suitable for downstream prediction tasks. In GNNs, gradients are propagated from the prediction layer back to GNN layers layer by layer. The model parameters in the GNN layers are updated based on the feedback from the downstream prediction task. In a fully parameterized way, a GNN can automatically extract an embedding vector for each vertex from its L-hop neighborhood, tuned according to the specific prediction task.

2.2. Graph Neuron and Message-passing Framework

Graph neurons are building blocks of a GNN. A GNN layer consists of $|\mathcal{V}|$ graph neurons. Each vertex corresponds to a graph neuron. A graph neuron is a small neural network. For the graph neuron corresponding to v_x at the layer l, it receives the hidden vector of itself $\boldsymbol{h}_x^l$ and the hidden vectors of its adjacent vertices $\boldsymbol{h}_y^l$ with $v_y \in \mathcal{N}(v_x)$ from the previous GNN layer[1]. The graph neuron of v_x aggregates the received hidden vectors, applies non-linear transformations, and outputs a new hidden vector $\boldsymbol{h}_x^{l+1}$.

We follow the message-passing framework [23] to formally define a graph neuron. The message-passing framework is widely used in the cutting-edge GNN libraries like PyG [14] and DGL [15]. Figure 2 shows the internal structure of a graph neuron in the message-passing framework. A graph neuron at the layer l are made of three *differentiable* functions: the messaging function ϕ^l, the aggregation function Σ^l, and the updating function γ^l.
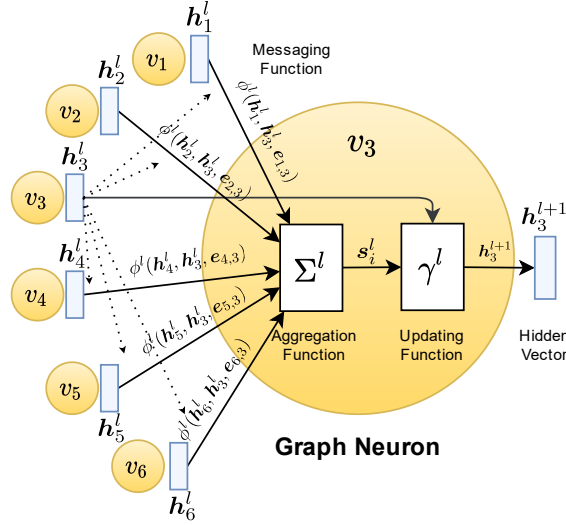

Figure 2: Graph neuron of v_3 in the GNN layer l with the demo graph $\mathcal{G}$ in Figure 1b. $\phi^l/\Sigma^l/\gamma^l$ are the messaging/aggregation/updating functions in the message-passing framework, respecitvely.

The graph neuron of v_x calculates the output hidden vector $\boldsymbol{h}_x^{l+1}$ with the three functions in three steps:

1. For every adjacent edge (v_y, v_x) of v_x ($v_y \in \mathcal{N}(v_x)$), the messaging function ϕ^l receives the output hidden vectors $\boldsymbol{h}_y^l$ and $\boldsymbol{h}_x^l$ from the previous GNN layer and the edge feature vector $\boldsymbol{e}_{y,x}$ (and other feature vectors associated with v_x/v_y if necessary) as the input. ϕ^l emits a *message vector* $\boldsymbol{m}_{y,x}^l$ for every edge (v_y, v_x) at the layer l, i.e. $\boldsymbol{m}_{y,x}^l = \phi^l(\boldsymbol{h}_y^l, \boldsymbol{h}_x^l, \boldsymbol{e}_{y,x}, \dots)$;

2. The aggregation function Σ^l then aggregates the message vectors $\boldsymbol{m}_{y,x}^l$ of the adjacent edges ($v_y \in \mathcal{N}(v_x)$) to produce an *aggregated vector* $\boldsymbol{s}_x^l$, i.e. $\boldsymbol{s}_x^l = \sum_{v_y \in \mathcal{N}(v_x)}^l \boldsymbol{m}_{y,x}^l$;

3. The updating function γ^l calculates the hidden vector of this layer $\boldsymbol{h}_x^{l+1}$ based on the hidden vector from the previous layer $\boldsymbol{h}_x^l$ and the aggregated vector $\boldsymbol{s}_x^l$ (and other feature vectors associated with v_x if necessary), i.e. $\boldsymbol{h}_x^{l+1} = \gamma^l(\boldsymbol{h}_x^l, \boldsymbol{s}_x^l, \dots)$.

Briefly, the behaviour of a graph neuron under the message-passing framework can be defined as

$$\boldsymbol{h}_x^{l+1} = \gamma^l(\boldsymbol{h}_x^l, \Sigma_{v_y \in \boldsymbol{N}(v_x)}^l \phi^l(\boldsymbol{h}_y^l, \boldsymbol{h}_x^l, \boldsymbol{e}_{y,x}, \dots), \dots). \tag{1}$$

The end-to-end training requires ϕ^l and γ^l (like multi-layer perceptrons and GRUs) and Σ^l (like mean, sum, element-wise min/max) are *differentiable* to make the whole GNN differentiable.

Different GNNs have different definitions of the three functions. We regard ϕ and Σ as *edge calculation* functions, since they are conducted over every edge in $\mathcal{G}$. We regard γ as the *vertex calculation* function, as

---

[1] For the GNN layer 0, graph neurons receive input feature vectors, i.e., $\boldsymbol{h}_x^0 = \boldsymbol{v}_x$

150 it is conducted over every vertex in $\mathcal{G}$. Table 2 and Table 3 list the edge calculation functions and the vertex calculation functions of typical GNNs, respectively. Some complex GNNs like GAT [6] and GaAN [7] use more than one message passing phase in each GNN layer. We regard every message passing phase in a GNN layer as a *sub-layer*. We will give out more details on sub-layers when we introduce GAT.

GNN	Type	Σ^l	$\phi^l(\boldsymbol{h}_y^l, \boldsymbol{h}_x^l, \boldsymbol{e}_{y,x}, \dots)$	Complexity
ChebNet [2]	Spectral	sum	$\boldsymbol{m}_{y,x}^l = \boldsymbol{e}_{y,x}\boldsymbol{h}_y^l$	$O(d_{in})$
GCN [1]	Spectral	sum	$\boldsymbol{m}_{y,x}^l = \boldsymbol{e}_{y,x}\boldsymbol{h}_y^l$	$O(d_{in})$
AGCN [3]	Spectral	sum	$\boldsymbol{m}_{y,x}^l = \tilde{e}_{y,x}^l\boldsymbol{h}_y^l$	$O(d_{in})$
GraphSAGE [5]	Non-spectral	mean/LSTM	$\boldsymbol{m}_{y,x}^l = \boldsymbol{h}_y^l$	$O(1)$
GraphSAGE-pool [5]	Non-spectral	max	$\boldsymbol{m}_{y,x}^l = \delta(\boldsymbol{W}_{pool}^l\boldsymbol{h}_y^l + b^l)$	$O(d_{in} * d_{out})$
Neural FPs [24]	Non-spectral	sum	$\boldsymbol{m}_{y,x}^l = \boldsymbol{h}_y^l$	$O(1)$
SSE [25]	Recurrent	sum	$\boldsymbol{m}_{y,x}^l = \boldsymbol{v}_y \parallel \boldsymbol{h}_y^l$	$O(f + d_{in})$
GGNN [4]	Gated	sum	$\boldsymbol{m}_{y,x}^l = \hat{\boldsymbol{h}}_y^l$	$O(1)$
GAT [6]	Attention	sum	Sub-layer 0:	concat: $O(d_{out})$
			$\boldsymbol{m}_{y,x}^{l,0} = \parallel_{k=1}^K \exp(LeakyReLU(\boldsymbol{a}^T[\hat{\boldsymbol{h}}_y[k] \parallel \hat{\boldsymbol{h}}_x[k]]))$	average: $O(K * d_{out})$
			Sub-layer 1 (multi-head concatenation):	Two Sub-layers
			$\boldsymbol{m}_{y,x}^{l,1} = \parallel_{k=1}^K \dfrac{\exp(LeakyReLU(\boldsymbol{a}^T[\hat{\boldsymbol{h}}_y[k] \parallel \hat{\boldsymbol{h}}_x[k]]))}{\boldsymbol{h}_x^{l,0}[k]}\hat{\boldsymbol{h}}_y[k]$	
			Sub-layer 1 (multi-head average) :	
			$\boldsymbol{m}_{j,i}^{l,1} = \dfrac{1}{K}\sum_{k=1}^K \dfrac{\exp(LeakyReLU(\boldsymbol{a}^T[\hat{\boldsymbol{h}}_y[k] \parallel \hat{\boldsymbol{h}}_x[k]]))}{\boldsymbol{h}_x^{l,0}[k]}\hat{\boldsymbol{h}}_y[k]$	
GaAN [7]	Attention	Sub-layer 0: sum	Sub-layer 0:	$O(\max(d_a, d_v, d_m) * K * d_{in})$
		Sub-layer 1: sum	$\boldsymbol{m}_{y,x}^{l,0} = \parallel_{k=1}^K \exp((\boldsymbol{W}_{(k),1}^l\boldsymbol{h}_y^l + \boldsymbol{b}_{(k),1}^l)^T(\boldsymbol{W}_{(k),2}^l\boldsymbol{h}_x^l + \boldsymbol{b}_{(k),2}^l))$	Four Sub-layers
		Sub-layer 2: max	Sub-layer 1:	$\boldsymbol{W}_{(k),1}^l \in \mathbb{R}^{d_a \times d_{in}}$
		Sub-layer 3: mean	$\alpha_{(k)} = \dfrac{\exp((\boldsymbol{W}_{(k),1}^l\boldsymbol{h}_y^l + \boldsymbol{b}_{(k),1}^l)^T(\boldsymbol{W}_{(k),2}^l\boldsymbol{h}_x^l + \boldsymbol{b}_{(k),2}^l))}{\boldsymbol{h}_x^{l,0}[k]}$	$\boldsymbol{W}_{(k),v}^l \in \mathbb{R}^{d_v \times d_{in}}$ $\boldsymbol{W}_m^l \in \mathbb{R}^{d_m \times d_{in}}$
			$\boldsymbol{m}_{y,x}^{l,1} = \parallel_{k=1}^K \alpha_{(k)} LeakyReLU(\boldsymbol{W}_{(k),v}^l\boldsymbol{h}_y^l + \boldsymbol{b}_{(k),v}^l)$	
			Sub-layer 2:	
			$\boldsymbol{m}_{y,x}^{l,2} = \boldsymbol{W}_m^l\boldsymbol{h}_y^l + \boldsymbol{b}_m^l$	
			Sub-layer 3:	
			$\boldsymbol{m}_{y,x}^{l,3} = \boldsymbol{h}_y^l$	

Table 2: Typical graph neural networks and their edge calculation functions. d_{in} and d_{out} are the dimensions of the input and output hidden vectors, respectively. Blue variables are model parameters to learn. δ is the activation function.

GNN	$\gamma^l(\boldsymbol{h}_x^l, \boldsymbol{s}_x^l, \dots)$	Complexity
ChebNet [2]	$\boldsymbol{h}_x^{l+1} = 2\boldsymbol{s}_x^l - \boldsymbol{h}_x^{l-1}$	$O(d_{out})$
GCN [1]	$\boldsymbol{h}_x^{l+1} = \boldsymbol{W}^l \boldsymbol{s}_x^l$	$O(d_{in} * d_{out})$
AGCN [3]	$\boldsymbol{h}_x^{l+1} = \boldsymbol{W}^l \boldsymbol{s}_x^l$	$O(d_{in} * d_{out})$
GraphSAGE [5]	$\boldsymbol{h}_x^{l+1} = \delta(\boldsymbol{W}^l[\boldsymbol{s}_x^l \parallel \boldsymbol{h}_x^l])$	$O(d_{in} * d_{out})$
GraphSAGE-pool [5]	$\boldsymbol{h}_x^{l+1} = \boldsymbol{s}_x^l$	$O(1)$
Neural FPs [24]	$\boldsymbol{h}_x^{l+1} = \delta(\boldsymbol{W}^{l,|\mathcal{N}(v_i)|}(\boldsymbol{h}_x^l + \boldsymbol{s}_x^l))$	$O(d_{in} * d_{out})$
SSE [25]	$\boldsymbol{h}_x^{l+1} = (1-\alpha)\boldsymbol{h}_x^l + \alpha\delta(\boldsymbol{W}_1^l\delta(\boldsymbol{W}_2^l[\boldsymbol{v}_x \parallel \boldsymbol{s}_x^l]))$	$O((f + d_{in}) * d_{out})$
GGNN [4]	Preprocessing: $\hat{\boldsymbol{h}}_x^l = \boldsymbol{W}^l \boldsymbol{h}_x^l$;	$O(d_{in} * d_{out})$
	$\boldsymbol{z}_x^l = \delta(\boldsymbol{W}^z \boldsymbol{s}_x^l + \boldsymbol{b}^{sz} + \boldsymbol{U}^z \boldsymbol{h}_x^l + \boldsymbol{b}^{hz})$	
	$\boldsymbol{r}_x^l = \delta(\boldsymbol{W}^r \boldsymbol{s}_x^l + \boldsymbol{b}^{sr} + \boldsymbol{U}^r \boldsymbol{h}_x^l + \boldsymbol{b}^{hr})$	
	$\bar{\boldsymbol{h}}_x^{l+1} = \tanh(\boldsymbol{W}\boldsymbol{s}_x^l + \boldsymbol{b}^s + \boldsymbol{U}(\boldsymbol{r}_x^l \odot \boldsymbol{h}_x^l) + \boldsymbol{b}^h)$	
	$\boldsymbol{h}_x^{l+1} = (1 - \boldsymbol{z}_x^l) \odot \boldsymbol{h}_x^l + \boldsymbol{z}_x^l \odot \bar{\boldsymbol{h}}_x^{l+1}$	
GAT [6]	Preprocessing: $\hat{\boldsymbol{h}}_x^l = \parallel_{k=1}^K \boldsymbol{W}_{(k)}^l \boldsymbol{h}_x^l$;	concat:$O(d_{in} * d_{out})$
	Sub-layer 0:	average:$O(K * d_{in} * d_{out})$
	$\boldsymbol{h}_x^{l,0} = \boldsymbol{s}_x^{l,0}$	Two Sub-layers
	Sub-layer 1:	
	$\boldsymbol{h}_x^{l+1} = \boldsymbol{h}_x^{l,1} = \delta(\boldsymbol{s}_x^{l,1})$	
		$O(\max(K * d_v + d_{in},$
GaAN [7]	Sub-layer 0/1/2:	$2 * d_{in} + d_m) * d_{out})$
	$\boldsymbol{h}_x^{l,*} = \boldsymbol{s}_x^{l,*}$	Four Sub-layers
	Sub-layer 3:	
	$\boldsymbol{g}_x^l = \boldsymbol{W}_g^l[\boldsymbol{h}_x^l \parallel \boldsymbol{h}_x^{l,2} \parallel \boldsymbol{s}_x^{l,3}] + \boldsymbol{b}_g^l$	
	$\boldsymbol{h}_x^{l+1} = \boldsymbol{h}_x^{l,3} = \boldsymbol{W}_o^l[\boldsymbol{h}_x^l \parallel (\boldsymbol{g}_x^l \odot \boldsymbol{h}_x^{l,1})] + \boldsymbol{b}_o^l$	

Table 3: Typical graph neural networks and their vertex calculation functions. d_{in} and d_{out} are the dimensions of the input and output hidden vectors, respectively. Blue variables are model parameters to learn. In Neural FPs, $\boldsymbol{W}^{l,|\mathcal{N}(i)|}$ is the weight matrix for vertices with degree $|\mathcal{N}(i)|$ at the layer l. δ is the activation function.

2.3. Representative GNNs

We use $O_\phi/O_\Sigma/O_\gamma$ to denote the time complexity of the three functions in the message-passing framework. The time complexity of a GNN layer is made up of two parts: the edge calculation complexity $O_\phi + O_\Sigma$ and the vertex calculation complexity O_γ. In Table 2 and Table 3, we list the edge and vertex calculation complexity of each GNN, respectively. The time complexity of a graph neuron is affected by the dimensions of the input/output hidden vectors d_{in} and d_{out} and the dimensions of the model parameters (like the number of heads K in GAT and the dimensions of the view vectors $d_a/d_v/d_m$ in GaAN).

Since we focus on analyzing the performance bottleneck in training GNNs, we classify the typical GNNs into four quadrants based on their edge/vertex complexity as shown in Figure 3. We pick GCN, GGNN, GAT, and GaAN as the *representative* GNNs of the four quadrants.

2.3.1. GCN (Low Vertex & Low Edge Complexity)

Graph convolution network (GCN [1]) introduces the first-order approximation of the spectral-based graph convolutions into graph neural networks. It has only one parameter to learn at each layer, i.e. the weight matrix $\boldsymbol{W}^l$ in the updating function γ^l. A GCN graph neuron can be expressed as $\boldsymbol{h}_x^{l+1} = \boldsymbol{W}^l \sum_{v_y \in \mathcal{N}(v_x)} w_{y,x} \boldsymbol{h}_y^l$, where $w_{y,x}$ is the normalized weight of the edge $e_{y,x}$. According to the associative law of the matrix multiplication, $\boldsymbol{h}_x^{l+1} = \sum_{v_y \in \mathcal{N}(v_x)} w_{y,x} \boldsymbol{W}^l \boldsymbol{h}_y^l$. Since the dimension of $\boldsymbol{h}_x^{l+1}$ is usually smaller than $\boldsymbol{h}_x^l$ in practical GCNs, the implementation of GCN in PyG chooses to first conduct the vertex calculation $\hat{\boldsymbol{h}}_y^l = \boldsymbol{W}^l \boldsymbol{h}_y^l$ for each vertex v_y and then conduct the edge calculation $\boldsymbol{h}_x^{l+1} = \sum_{v_y \in \mathcal{N}(v_x)} w_{y,x} \hat{\boldsymbol{h}}_y^l$. As $\hat{\boldsymbol{h}}_y^l$ has the same dimension as $\boldsymbol{h}_x^{l+1}$, the implementation significantly reduces the computation cost of the edge calculation.

2.3.2. GGNN (High Vertex & Low Edge Complexity)

GGNN [4] introduces the gated recurrent unit (GRU) into graph neural networks. The updating function γ^l of GGNN is a modified GRU unit that has 12 model parameters to learn, having high computational complexity. To lower the training cost, all GNN layers share the same group of parameters in GGNN. GGNN further requires
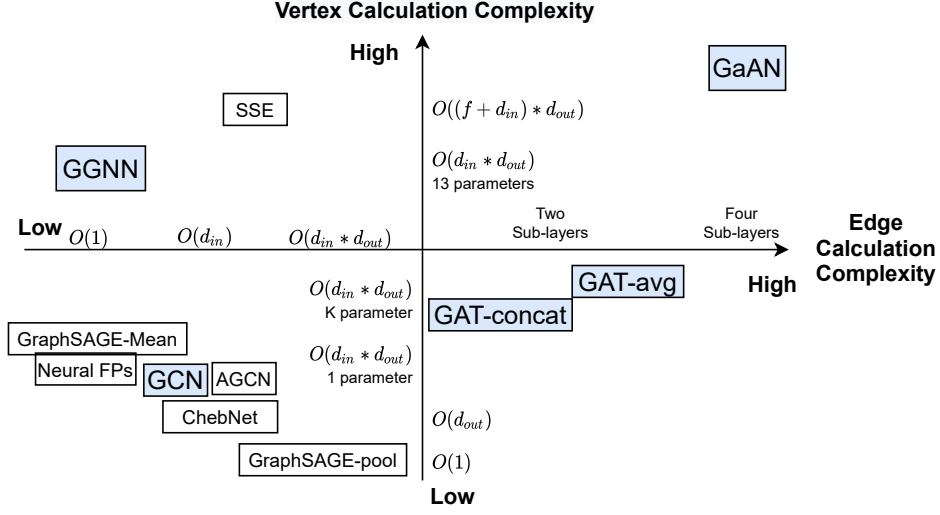
Figure 3: Complexity quadrants of typical GNNs. We compare the complexity according to the number of sub-layers, the Big-O notation, and the number of parameters to train.

the dimension of $\boldsymbol{h}^{l+1}$ is equal to the dimension of $\boldsymbol{h}^l$. Since the messaging function ϕ^l only uses the hidden vector $\boldsymbol{h}_y^l$ of the source vertex v_y for an edge $e_{y,x}$, in the implementation of PyG, GGNN conducts the pre-processing vertex calculation $\hat{\boldsymbol{h}}_x^l = \boldsymbol{W}^l \boldsymbol{h}_x^l$ for every vertex v_x before the message passing. The messaging function ϕ^l directly uses $\hat{\boldsymbol{h}}_y^l$ as the message vector for every edge $e_{y,x}$. In this way, GGNN further reduces the time complexity of the edge calculation to $O(1)$ without increasing the time complexity of the vertex calculation.

2.3.3. GAT (Low Vertex & High Edge Complexity)

GAT [6] introduces the multi-head attention mechanism into graph neural networks. Each GAT layer has K heads that generate K independent views for an edge, where K is a hyper-parameter. The views of K heads can be merged by concatenating or by averaging. For concatenating, the dimension of the hidden vector of each head d_{head} is d_{out}/K. For averaging, d_{head} is d_{out}.

Each GAT layer consists of a vertex pre-processing phase and two sub-layers (i.e., message-passing phases).

The vertex pre-processing phase calculates the attention vector $\hat{\boldsymbol{h}}_x^l$ for every vertex v_x by $\hat{\boldsymbol{h}}_x = \|_{k=1}^K \boldsymbol{W}_{(k)}^l \boldsymbol{h}_x^l$. We denote the attention sub-vector generated by the k-th head as $\hat{\boldsymbol{h}}_x[k] = \boldsymbol{W}_{(k)}^l \boldsymbol{h}_x^l$.

The first sub-layer of GAT (defined in Equation 2) uses the attention vectors to emit the attention weight vector $\boldsymbol{m}_{y,x}^{l,0}$ for every edge $e_{y,x}$ and aggregates the attention weight vectors for every vertex v_x to get the weight sum vector $\boldsymbol{h}_x^{l,0}$.

$$
\begin{aligned}
\boldsymbol{m}_{y,x}^{l,0} &= \phi^{l,0}(\boldsymbol{h}_y^l, \boldsymbol{h}_x^l, \boldsymbol{e}_{y,x}, \hat{\boldsymbol{h}}_y, \hat{\boldsymbol{h}}_x) = \|_{k=1}^K \exp(LeakyReLU(\boldsymbol{a}^T[\hat{\boldsymbol{h}}_y[k] \| \hat{\boldsymbol{h}}_x[k]])), \\
\boldsymbol{s}_x^{l,0} &= \sum_{v_y \in \mathcal{N}(v_x)} \boldsymbol{m}_{y,x}^{l,0}, \\
\boldsymbol{h}_x^{l,0} &= \gamma^{l,0}(\boldsymbol{h}_x^l, \boldsymbol{s}_x^{l,0}) = \boldsymbol{s}_x^{l,0}.
\end{aligned}
\tag{2}
$$

The second sub-layer of GAT (defined in Equation 3) uses the weight sum vectors to normalize the attention weights for every edge and aggregates the attention vectors $\hat{\boldsymbol{h}}_y^l$ with the normalized weights. The aggregated attention vectors $\boldsymbol{s}_x^{l,1}$ are transformed by an activation function δ and are outputted as the hidden vectors of the current layer $\boldsymbol{h}_x^{l+1}$.

$$
\begin{aligned}
\boldsymbol{m}_{y,x}^{l,1} &= \phi^{l,1}(\boldsymbol{h}_y^{l,0}, \boldsymbol{h}_x^{l,0}, \boldsymbol{e}_{y,x}, \hat{\boldsymbol{h}}_y, \hat{\boldsymbol{h}}_x) = \|_{k=1}^K \frac{\exp(LeakyReLU(\boldsymbol{a}^T[\hat{\boldsymbol{h}}_y[k] \| \hat{\boldsymbol{h}}_x[k]]))}{\boldsymbol{h}_x^{l,0}[k]} \hat{\boldsymbol{h}}_y[k], \\
\boldsymbol{s}_x^{l,1} &= \sum_{v_y \in \mathcal{N}(v_x)} \boldsymbol{m}_{y,x}^{l,1}, \\
\boldsymbol{h}_x^{l+1} = \boldsymbol{h}_x^{l,1} &= \gamma^{l,1}(\boldsymbol{h}^{l,0}, \boldsymbol{s}_x^{l,1}) = \delta(\boldsymbol{s}_x^{l,1}).
\end{aligned}
\tag{3}
$$

8

2.3.4. GaAN (High Vertex & High Edge Complexity)

Based on the multi-head mechanism, GaAN [7] introduces a convolutional subnetwork to control the weight of each head. Each GaAN layer consists of four sub-layers (as defined in Table 2 and Table 3). The first two sub-layers are similar to GAT, and the last two sub-layers build the convolutional subnetwork. The first sub-layer aims to get the sum of attention weights of every vertex in all heads $\boldsymbol{h}_x^{l,0}$. The second sub-layer aggregates the hidden vectors from the previous GaAN layer with the normalized attention weights for all heads $\alpha_{(k)}$. The third and fourth sub-layers aggregate the hidden vectors from the GaAN previous layer with the element-wise max and mean operators separately. The vertex updating funciton $\gamma^{l,3}$ of the fourth sub-layer uses the hidden vectors of the last two sub-layers $\boldsymbol{h}_x^{l,1}, \boldsymbol{h}_x^{l,2}$ to generate the output hidden vector $\boldsymbol{h}_x^{l+1}$.

2.4. Sampling Techniques

By default, GNNs are trained in a full-batch way, using the whole graph in each iteration. But the full-batch gradient descent has two disadvantages [26]: (1) it has to cache intermediate results of all vertices in the forward phase, consuming lots of memory space, which is not scalable; (2) it updates the model parameters only once for each epoch, slowing the convergence of gradient descent.

To train GNNs in a mini-batch way, the sampling techniques [5, 27, 28, 29, 30, 26, 31] are proposed. In each mini-batch, they sample a small subgraph from the whole graph $\mathcal{G}$ and uses the subgraph to update the model parameters. The sampling techniques only activate the graph neurons and the connections that appear in the sampled subgraph between GNN layers, as shown in Figure 4. Inactive graph neurons and connections do not participate in the training of this mini-batch, saving lots of computation and storage costs. Moreover, it may reduce the risk of overfitting the training graph. The existing sampling techniques can be classified into two groups: *neighbor sampling* and *graph sampling*, based on whether different GNN layers sample different subgraphs.

The neighbor sampling techniques [5, 27, 28, 29, 32] sample nodes or edges layer by layer. The sampled subgraphs of different GNN layers may be *different*, as shown in Figure 4(a). GraphSAGE [5] is a representative neighbor sampling technique. The technique first samples several vertices from $\mathcal{V}$ in the last GNN layer. Then it repeatedly samples the neighbors of the sampled vertices from the previous layer until the input layer. For every sampled vertex v_x in the GNN layer l, GraphSAGE samples at most η^l neighbors of v_x from the previous layer. η^l is the hyper-parameter that is usually small. In this way, GraphSAGE limits neighborhood sizes of vertices in the sampled subgraph, especially high-degree vertices.
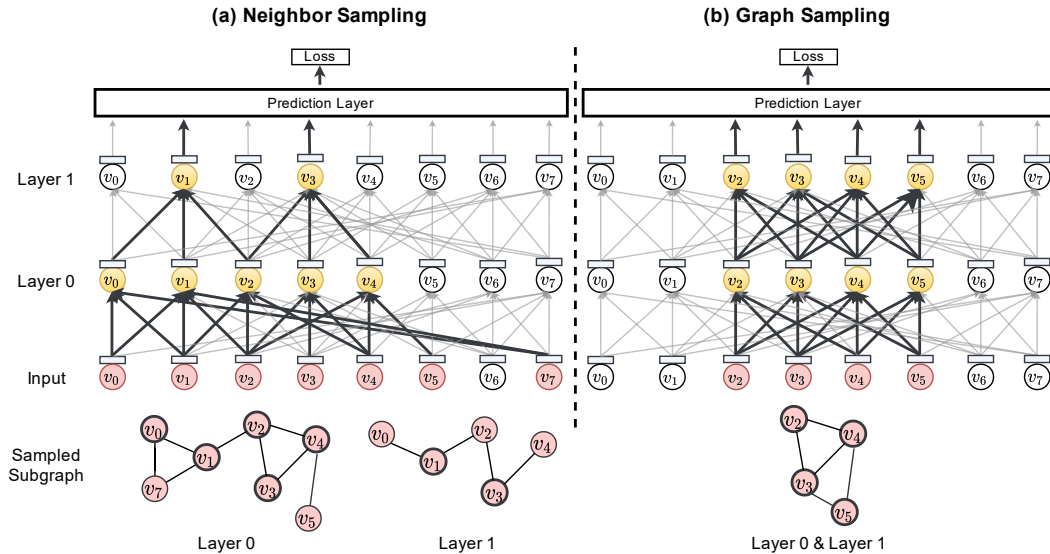

Figure 4: Training a GNN with sampling techniques. The faded graph neurons and their connections are inactivated.

The graph sampling techniques [30, 26, 31] sample a subgraph for each mini-batch and use the same sampled subgraph for all GNN layers, as shown in Figure 4(b). They differ in how to sample subgraphs. The cluster sampler technique [26] is a representative graph sampling technique. Given a training graph $\mathcal{G}$, it partitions $\mathcal{G}$

into several dense clusters. For each mini-batch, it randomly picks N clusters to form the sampled subgraph, where N is the hyper-parameter.

In the implementation in PyG, the model parameters of GNNs reside on the GPU side and the input graph resides on the host side. To process an epoch, PyG samples the original graph in the main memory and generates several batches for the epoch. For each batch, PyG sends the sampled subgraph to the GPU, propagates the feature vectors of the sampled subgraph from the input layer to the prediction layer, calculates the gradients on the subgraph, and updates the model parameters based on the gradients directly on the GPU. With the sampling techniques, the model parameters are updated by a stochastic gradient descent optimizer. PyG conducts the evaluation phase every several epochs or batches (either on the CPU side or the GPU side) to determine whether to stop the training.

2.5. Inference with GNNs

The model parameters of a GNN consist of the weight vectors/matrices in the prediction layer and the messaging/aggregation/updating functions of each GNN layer. For transductive learning, the input graphs of training and inference are the same. The structure of the GNN does not need to adjust. For inductive learning, the input graphs used in training and inference are different. When we want to perform inference on a new graph with a pre-trained GNN, the structure of the GNN needs to be adjusted, but the hyper-parameters and the model parameters of the GNN remain unchanged. The number of graph neurons in each GNN layer has to be adjusted to $|\mathcal{V}|$ of the new graph. The connections of graph neurons between GNN layers are also adjusted according to the edge set of the new graph. During inference, input feature vectors of the input graph are propagated forward from the input layer to the prediction layer to give out predicted labels.

When the memory capacity of the GPU is large enough to hold all of the input graph and intermediate results during inference, the inference can produce predicted labels for all vertices and edges at once, making full use of the computing power of the GPU. When the memory capacity is not large enough, the sampling technique must be adopted.

The sample-based inference splits the test set into several batches. For each batch, the sample-based inference samples a subgraph related to the batch from the input graph. It performs inference on the sampled subgraph to produce predicted labels for the batch. Since the sampled subgraph is usually much smaller than the original input graph, the memory usage during inference is limited. The sampling method depends on the prediction task. Taking the node classification task as an example, if there are L GNN layers in the GNN, the hidden vector outputted by the last GNN layer of each vertex $\boldsymbol{h}_x^L$ is only related to the L-hop neighborhood of v_x. Thus, if we want to predict labels for a group of vertices, we only need to sample a subgraph that contains L-hop neighborhoods of all given vertices.

The implementation of sample-based inference in PyG stores the whole input graph and its feature vectors in the main memory. In the node classification task, it splits the vertices in the test set into batches according to the given batch size. The subgraph corresponding to each batch is sampled on the CPU side and sent to the GPU side to perform inference.

3. Evaluation Design

We design a series of experiments to explore the performance bottleneck in training graph neural networks. We first introduce our experimental setting in Section 3.1 and then give out our experimental scheme in Section 3.2. The evaluation results are presented and analyzed later in Section 4.

3.1. Experimental Setting

Experimental Environment. All the experiments were conducted in a CentOS 7 server with the Linux kernel version 3.10.0. The server had 40 cores and 90 GB main memory. The server was equipped with an NVIDIA Tesla T4 GPU card with 16GB GDDR6 memory. For the software environment, we adopted Python 3.7.7, PyTorch 1.5.0, and CUDA 10.1. We implemented all GNNs with PyG 1.5.0[2].

---

[2]https://pytorch-geometric.readthedocs.io/en/1.5.0/index.html

Learning Task. We used the node classification as the target task in GNNs due to its popularity in real-world applications. We trained GNNs in the semi-supervised learning setting. All vertices and their input feature vectors were used, but only a part of the vertices was attached with labels during the training and they were used to calculate the loss and gradients. The vertices with unseen labels were used in the evaluation and inference phase to evaluate the accuracy of GNN models.

Datasets. We used six real-world graph datasets as listed in Table 4 that were popular in the GNN accuracy evaluation [28, 31, 33, 34]. For directed graphs, PyG converted them into undirected ones during data loading. Thus, the average degree of a directed graph $\bar{d} = \frac{2|\mathcal{E}|}{|\mathcal{V}|}$. For an undirected graph, the average degree was defined as $\bar{d} = \frac{|\mathcal{E}|}{|\mathcal{V}|}$. For the `cam` dataset, its vertices were not associated with feature vectors. Thus, we generated random dense feature vectors for it and excluded it from accuracy evaluation. For `amp`, `amc`, `cph`, and `cam`, we used 70%/15%/15% of the samples as the training/evaluation/test set, respectively. For `pub`, we used 500/1000 vertices as the evaluation/test set and the remained as the training set according to [28]. For `fli`, we used 50%/25%/25% of the samples as the training/evaluation/test set according to [31]. We also used random graphs generated by the R-MAT graph generator [35] in some experiments, to explore the effects of graph topological characteristics (like average degrees) on performance bottlenecks. Input feature vectors of random graphs were random dense vectors with a dimension of 32. Vertices of random graphs were classified into 10 classes randomly.

Dataset	$\lvert\mathcal{V}\rvert$	$\lvert\mathcal{E}\rvert$	$\bar{d}$	$dim(\boldsymbol{v})$	#Class	Directed
pubmed (`pub`) [28]	19,717	44,324	4.5	500	3	Yes
amazon-photo (`amp`) [33]	7,650	119,081	31.1	745	8	Yes
amazon-computers (`amc`) [33]	13,752	245,861	35.8	767	10	Yes
coauthor-physics (`cph`) [33]	34,493	247,962	14.4	8415	5	Yes
flickr (`fli`) [31]	89,250	899,756	10.1	500	7	No
com-amazon (`cam`) [34]	334,863	925,872	2.8	32	10	No

Table 4: Dataset overview. $\bar{d}$ represents the average vertex degree. $dim(\boldsymbol{v})$ is the dimension of the input feature vector.

GNN Implementation. We implemented the four typical GNNs: GCN, GGNN, GAT, and GaAN. To compare performance characteristics of the four GNNs side-by-side, we used a unified GNN structure for them: Input Layer → GNN Layer 0 → GNN Layer 1 → Softmax Layer (to prediction). The structure was popular in the experimental evaluation of GCN [1], GAT [6], and GaAN [7]. Since a GGNN layer required the input and output hidden vectors had the same dimension, we added two multi-layer perceptron (MLP) layers to transform the dimensions of the input/output feature vectors: Input Layer → MLP → GGNN Layer 0 → GGNN Layer 1 → MLP → Softmax Layer. Unless otherwise specified, we stored the dataset and the model parameters on the GPU side. The GNN training was conducted also on the GPU side.

Hyper-parameters. We used $dim(\boldsymbol{x})$ to denote the dimension of a vector $\boldsymbol{x}$. We picked the hyper-parameters of GNNs according to their popularity in their references [1, 4, 6, 7]. Unless otherwise mentioned, we used the same set of hyper-parameters for all the datasets. Some hyper-parameters (like dimensions of hidden vectors) were common in the four GNNs and we set them to the same values. For GCN/GAT/GaAN, we set $\boldsymbol{h}_x^0 = \boldsymbol{v}_x$, $dim(\boldsymbol{h}_x^1) = 64$, and $dim(\boldsymbol{h}_x^2) = \#Class$ (the number of classes in the dataset). For GAT, the first GAT layer contained 8 heads, and the attention vector of each head had a dimension of 8. The first GAT layer merged attention vectors of 8 heads by concatenating. The second GAT layer used a single head with a dimension of $\#Class$. For GGNN, we set $dim(\boldsymbol{h}_x^0) = dim(\boldsymbol{h}_x^1) = dim(\boldsymbol{h}_x^2) = 64$. We used 8 heads in the both GaAN layers with $d_a = d_v = 8$, and $d_m = 64$.

We used Adam [36] as the gradient descent optimizer with a learning rate of 0.01 and a weight decay of 1e-5. We initialized weights in GNNs using the method described in [37] and initialized bias as zeros. Without otherwise mentioned, in the experiments related to accuracy evaluation, we trained all GNNs for a maximum of 100k epochs and used the early stopping criterion according to [33]: the training was stopped if the validation loss did not improve for 50 epochs. We chose the model parameters that achieved the lowest validation loss as the final model parameters. The accuracy of the test set was evaluated with the final model.

Sampling Techniques. We picked the neighbor sampler from GraphSAGE [5] and the cluster sampler from ClusterGCN [26] as the typical sampling techniques. For the neighbor sampler, we set the neighborhood sample sizes of the GNN layer 0 and the GNN layer 1 to 10 and 25, respectively. We set the default batch size to 512, according to [5]. For the cluster sampler, we partitioned the input graph into 1500 partitions and used 20 partitions per batch, according to [26].

3.2. Experimental Scheme

To find out performance bottlenecks in GNN training, we conducted the experimental analysis with four questions. The answers to those questions would give us a more comprehensive view of the performance characteristics of GNN training.

Q1 *How did the hyper-parameters affect the training/inference time, memory usage and accuracy of a GNN?* (Section 4.1)

Every GNN had a group of hyper-parameters, such as the number of GNN layers and the dimensions of hidden feature vectors. The hyper-parameters affected the processing time per epoch and peak memory usage during training and inference. They also affected the accuracy of a GNN. Larger hyper-parameter values usually meant more model parameters and more complex models. To evaluate their effects, we measured the training/inference time per epoch, the peak memory usage (of the GPU), and the test accuracy changed as we increased the values of the hyper-parameters. Through the experiments, we verified the validity of the time complexity analysis in Table 2 and Table 3. The complexity analysis allowed us to analyze performance bottlenecks theoretically.

Q2 *Which stage was the most time-consuming stage in GNN training and inference?* (Section 4.2)

We decomposed the GNN training/inference time on different levels: the layer level, the edge/vertex calculation level, and the basic operator level. On each level, we decomposed the time of an epoch into several stages. The most time-consuming stage was the performance bottleneck. Optimizing its implementation would significantly reduce the training time.

Q3 *Which consumed most of memory in GNN training and inference?* (Section 4.3)

The limited memory capacity of a GPU prevented us from conducting training/inference on big graphs. We measured the peak memory usage during GNN training/inference under different graph scales, input feature dimensions, and average degrees. Based on the results, we analyzed which was the most memory-consuming component in a GNN. Reducing its memory usage would enable us to train GNNs on bigger graphs under the same memory capacity.

Q4 *Could sampling techniques remove performance bottlenecks in GNN training/inference? Did the use of sampling techniques in training sacrifice model accuracy?* (Section 4.4)

Theoretically, sampling techniques could significantly reduce the number of graph neurons that participated in the training of a batch. Consequently, the processing time and memory usage per batch should also decrease. The model accuracy of GNNs might also be affected. To validate the effectiveness of sampling techniques, we measured the training/inference time, peak memory usage, and test accuracy under different batch sizes. If sampling techniques were effective, they would be the keys to conduct GNN training/inference on very big graphs. If they were not effective, we wanted to find out which impaired their efficiency.

4. Evaluation Results and Analysis

We answer the four questions in Section 3.2 one by one with experiments. Without otherwise mentioned, the reported training time per epoch was the average wall-clock training time of 50 epochs, excluding abnormal epochs. During the training of some epochs, there were extra profiling overheads from NVIDIA Nsight Systems and GC pauses from the Python interpreter that significantly increased the training time. We denoted the 25% and 75% quantiles of the training time of 50 epochs as Q1 and Q3, respectively. We regarded the epochs with the training time *outside* the range of $[Q1 - 1.5 * (Q3 - Q1), Q3 + 1.5 * (Q3 - Q1)]$ as abnormal epochs.

4.1. Effects of Hyper-parameters on Performance

The hyper-parameters of a GNN (such as the dimensions of hidden vectors and the number of heads) determined the model complexity of the GNN. They affected the training/inference time, memory usage, and accuracy of the GNN at the same time.

4.1.1. Effects on Training Time

According to Table 2 and Table 3, the time complexity of the messaging function ϕ and the updating function γ was linear to each hyper-parameter separately. If we increased one of the hyper-parameters and fixed the others, the training time should increase linearly in theory.

To verify the time complexity analysis in Table 2 and Table 3, we first compared the training time of the four GNNs in Figure 5. The ranking of the training time was GaAN $\gg$ GAT > GGNN > GCN in all cases. Since the real-world graphs had more edges than vertices ($|\mathcal{E}| > |\mathcal{V}|$), the time complexity of the edge calculation stage affected more obviously than the vertex calculation stage. The ranking was consistent with the time complexity analysis.
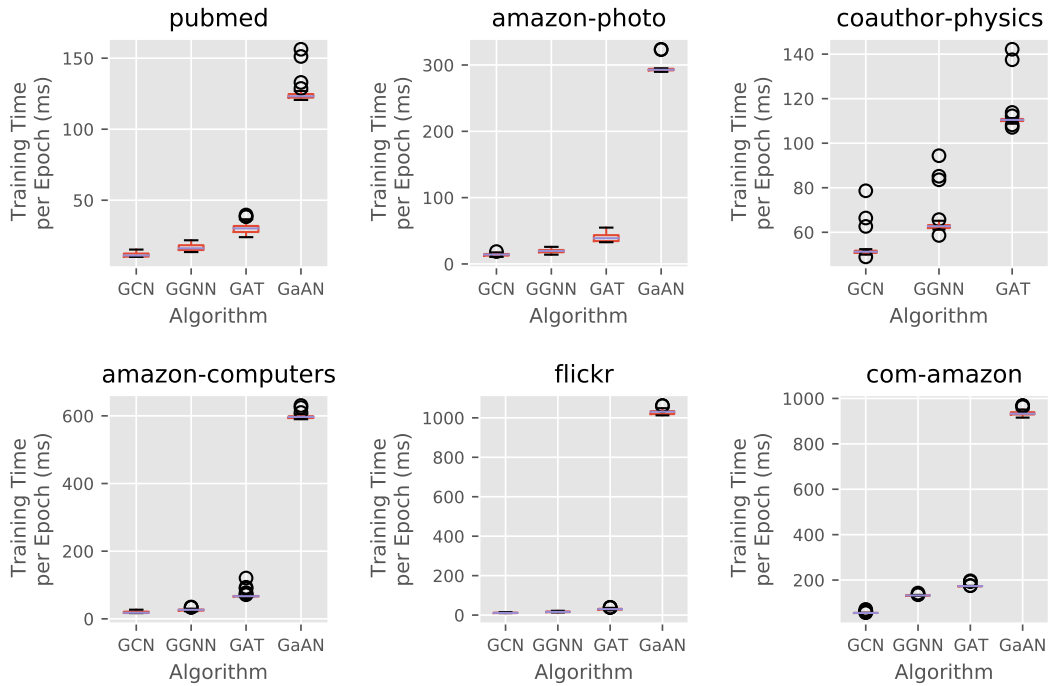
Figure 5: Distribution of the wall-clock training time of 50 epochs on different datasets. GaAN crashed due to the out of memory exception on the `cph` dataset.

To further evaluate effects of hyper-parameters on training time, we measured the training time of each GNN with varying hyper-parameters in Figure 6 to Figure 9.

For GCN and GGNN, $dim(\boldsymbol{h}_x^0)$ and $dim(\boldsymbol{h}_x^1)$ were solely determined by the dataset with $d_{in}^0 = dim(\boldsymbol{h}_x^0) = dim(\boldsymbol{v_x})$ and $d_{out}^1 = dim(\boldsymbol{h}_x^2) = \#Class$. Therefore, the only modifiable hyper-parameter was the dimension of $\boldsymbol{h}_x^1$ that affected the dimension of output hidden vectors of the layer 0 d_{out}^0 and the dimension of input hidden vectors of the layer 1 d_{in}^1 simultaneously, i.e. $dim(\boldsymbol{h}_x^1) = d_{out}^0 = d_{in}^1$. According to the time complexity analysis, if we fixed other hyper-parameters but only increased $dim(\boldsymbol{h}_x^1)$, the computational costs of the GNN layer 0 and the GNN layer 1 should both increase linearly with $dim(\boldsymbol{h}_x^1)$, causing the training time of the whole GNN also increased linearly. Figure 6 and Figure 7 show that the training time of GCN and GGNN increased linearly with $dim(\boldsymbol{h}_x^1)$ when $dim(\boldsymbol{h}_x^1)$ was big, consistent with the theoretical analysis.

13
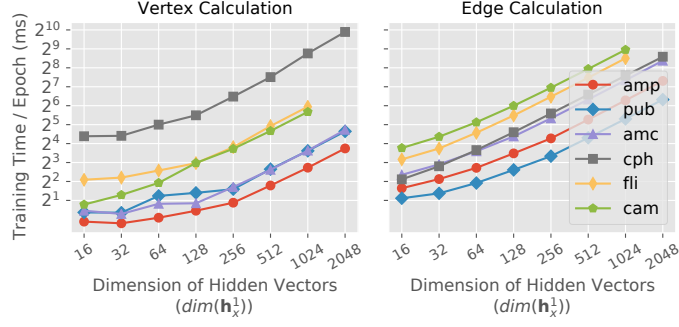
Figure 6: Effects of hyper-parameters on the vertex/edge calculation time of GCN in training.
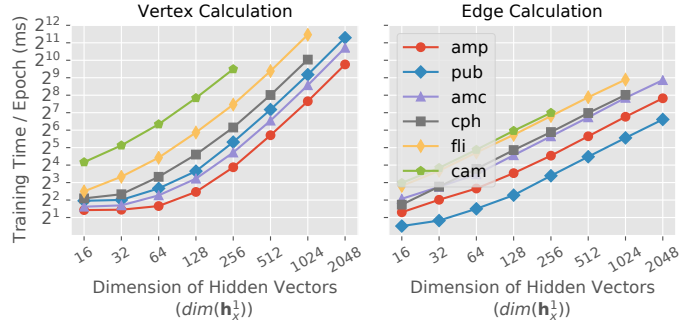
Figure 7: Effects of hyper-parameters on the vertex/edge calculation time of GGNN in training.

For GAT, we modified the number of heads K and the dimension of each head d_{head} in the GAT layer 0. The dimension of $\boldsymbol{h}_x^1$ was determined as $dim(\boldsymbol{h}_x^1) = Kd_{head}$. Thus, the computational costs of the GAT layer 0 and the GAT layer 1 should increase linearly with K and d_{head} separately. Figure 8 confirms the theoretical analysis.
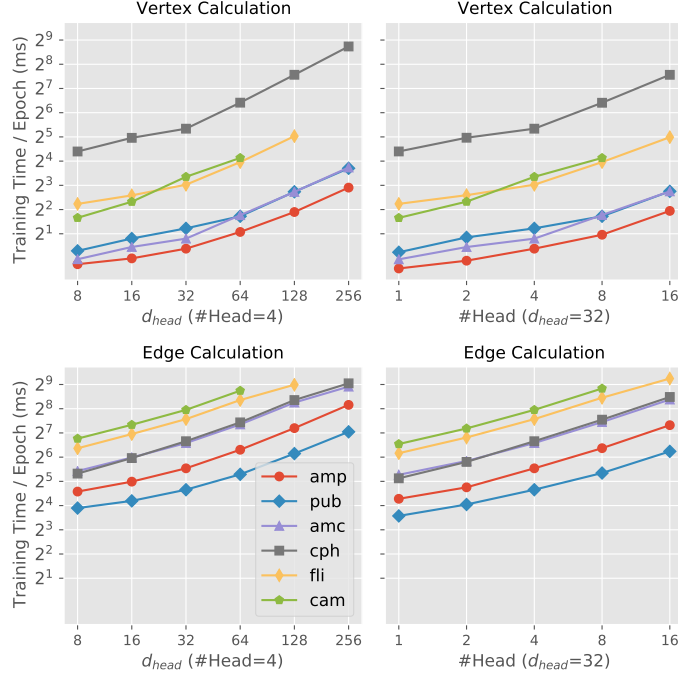
Figure 8: Effects of hyper-parameters on the vertex/edge calculation time of GAT in training.

For GaAN, it was also based on the multi-head mechanism. Its time complexity should be affected by $dim(\boldsymbol{h}_x^1)$ ($d_{out}^0 = d_{in}^1 = dim(\boldsymbol{h}_x^1)$), d_a, d_v, d_m, and the number of heads K. Figure 9 demonstrates that the training time increased linearly with the hyper-parameters, except for $dim(\boldsymbol{h}_x^1)$. As $dim(\boldsymbol{h}_x^1)$ increased, the training time increased first slightly and then linearly. We observed similar phenomena in GCN, GGNN, and GAT: When the values of hyper-parameters were too low, GNN training could not make full use of the computing power of the GPU. When the values of hyper-parameters became high enough, training time increased linearly, supporting the time complexity analysis.

15
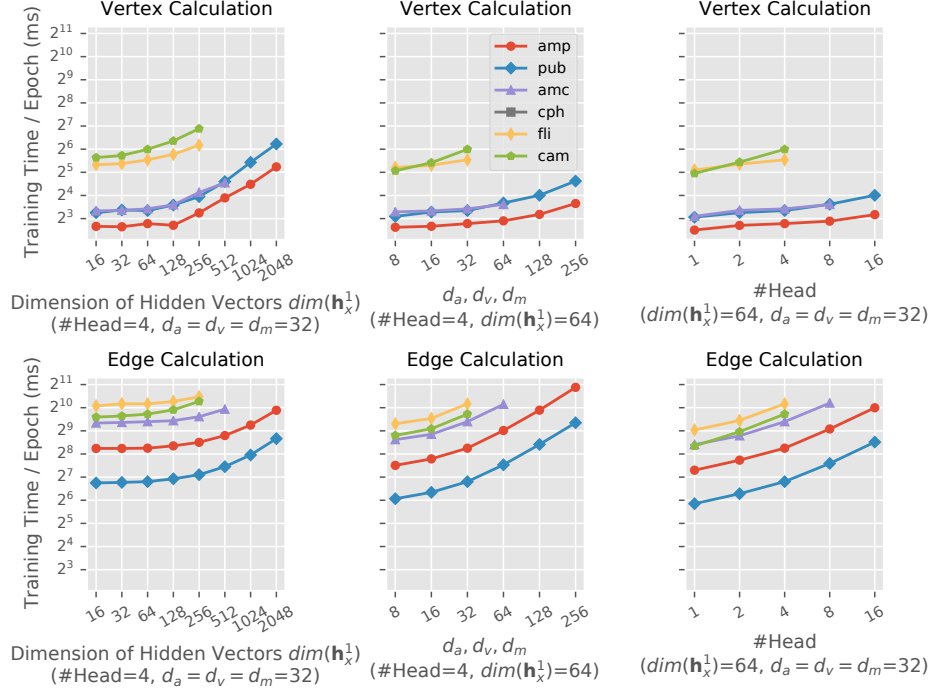
Figure 9: Effects of hyper-parameters on the vertex/edge calculation time of GaAN in training.

4.1.2. Effects on Inference Time

For all GNNs, we found that the effects of hyper-parameters on the inference time were the same as the training time. Taking GGNN as an exmple, Figure 10 shows the effects of hyper-parameters on the inference time of GGNN. By cross-comparing Figure 10 and Figure 7, the trends of the inference time and training time were the same: as $dim(\boldsymbol{h}_x^1)$ increased, the vertex and edge calculation time both grew linearly when $dim(\boldsymbol{h}_x^1)$ was large enough. For the other GNNs, we observed similar phenomena. The results indicated that the complexity analysis presented in Table 2 and Table 3 were also applicable to inference.
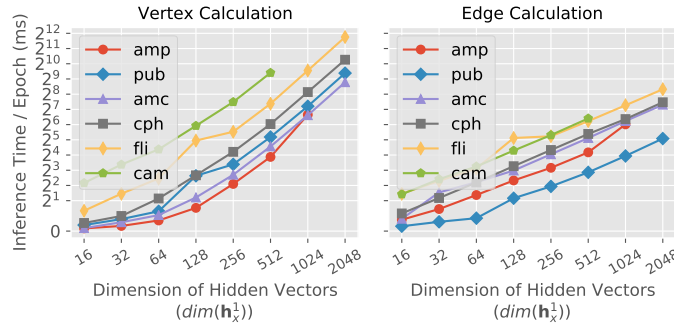
Figure 10: Effects of hyper-parameters on the vertex/edge calculation time of GGNN in inference.

4.1.3. Effects on Peak Memory Usage

We further measured the effects of hyper-parameters on the peak GPU memory usage during training in Figure 11. The memory usage also increased linearly as the hyper-parameters increased for all GNNs, except for GaAN on $dim(\boldsymbol{h}_x^1)$. As the hidden vectors $\boldsymbol{h}_x^1$ in GaAN consumed a small proportion of memory, the growth in the memory usage was not noticeable until $dim(\boldsymbol{h}_x^1)$ was large enough. The effects of hyper-parameters on the inference memory usage were the same as the training. Taking GAT as an example, Figure 12 shows that the peak memory usage during inference grew linearly with the increasing hyper-parameters. By cross-comparing

16

Figure 12 and Figure 11c, the hyper-parameters affected the peak memory usage of training and inference in the same way. For the other GNNs, we observed similar phenomena.

(a) GCN   (b) GGNN   (c) GAT

(d) GaAN
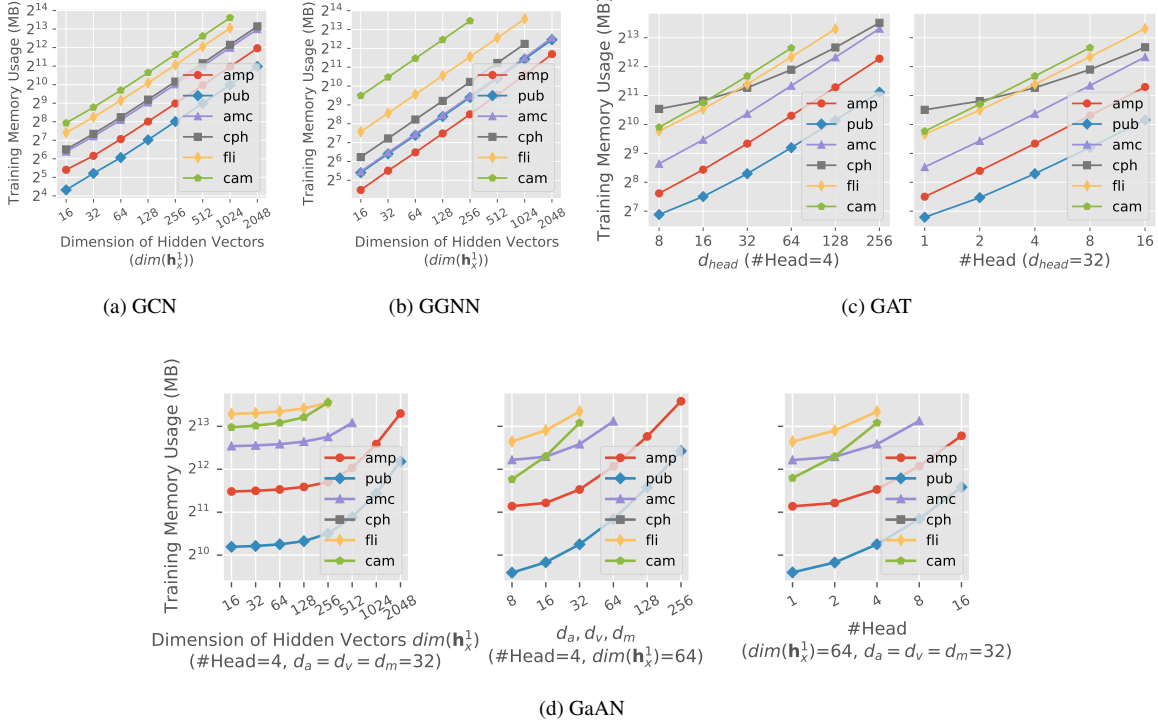
Figure 11: Effects of hyper-parameters on the peak GPU memory usage during training, excluding the memory used by the dataset and the model parameters.
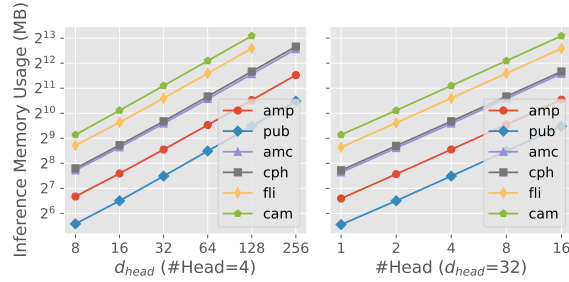
Figure 12: Effects of hyper-parameters on the peak GPU memory usage during inference of GAT, excluding the memory used by the dataset and the model parameters.

4.1.4. Effects on Accuracy

The values of hyper-parameters determined the model complexity of a GNN. The relationships between model complexity and accuracy were complex. Generally speaking, higher model complexity brought more powerful representation capability and might bring higher accuracy, but it also increased the risk of overfitting.

To evaluate the effects of hyper-parameters on accuracy, we measured the accuracy of the typical GNNs with varying hyper-parameters in Figure 13. For GCN, its accuracy was sensitive to the dimension of hidden vectors $dim(\boldsymbol{h}_x^1)$. As $dim(\boldsymbol{h}_x^1)$ increased, the accuracy first increased quickly and then stabilized when $dim(\boldsymbol{h}_x^1) \geq 8$. For GGNN, its accuracy curves showed similar trends as GCN, but GGNN was more sensitive to $dim(\boldsymbol{h}_x^1)$ than GCN. Its accuracy even decreased when $dim(\boldsymbol{h}_x^1) \geq 1024$. Since the model complexity of GGNN was high

17

(with 13 weight matrices/vectors to train), GGNN might occur overfitting in those cases. For GAT, its accuracy was more sensitive to the dimension of each head d_{head} than the number of heads. For GaAN, only $dim(\boldsymbol{h}_x^1)$ showed obvious impacts on accuracy. The experimental results indicated that the accuracy of the GNNs was often low when $dim(\boldsymbol{h}_x^1)$ (for GCN/GGNN/GaAN) or d_{head} (for GAT) was very low. As $dim(\boldsymbol{h}_x^1)$ or d_{head} increased to a certain threshold, the GNNs gained sufficient learning ability to achieve stable accuracy.

(a) GCN   (b) GGNN

(c) GAT

(d) GaAN
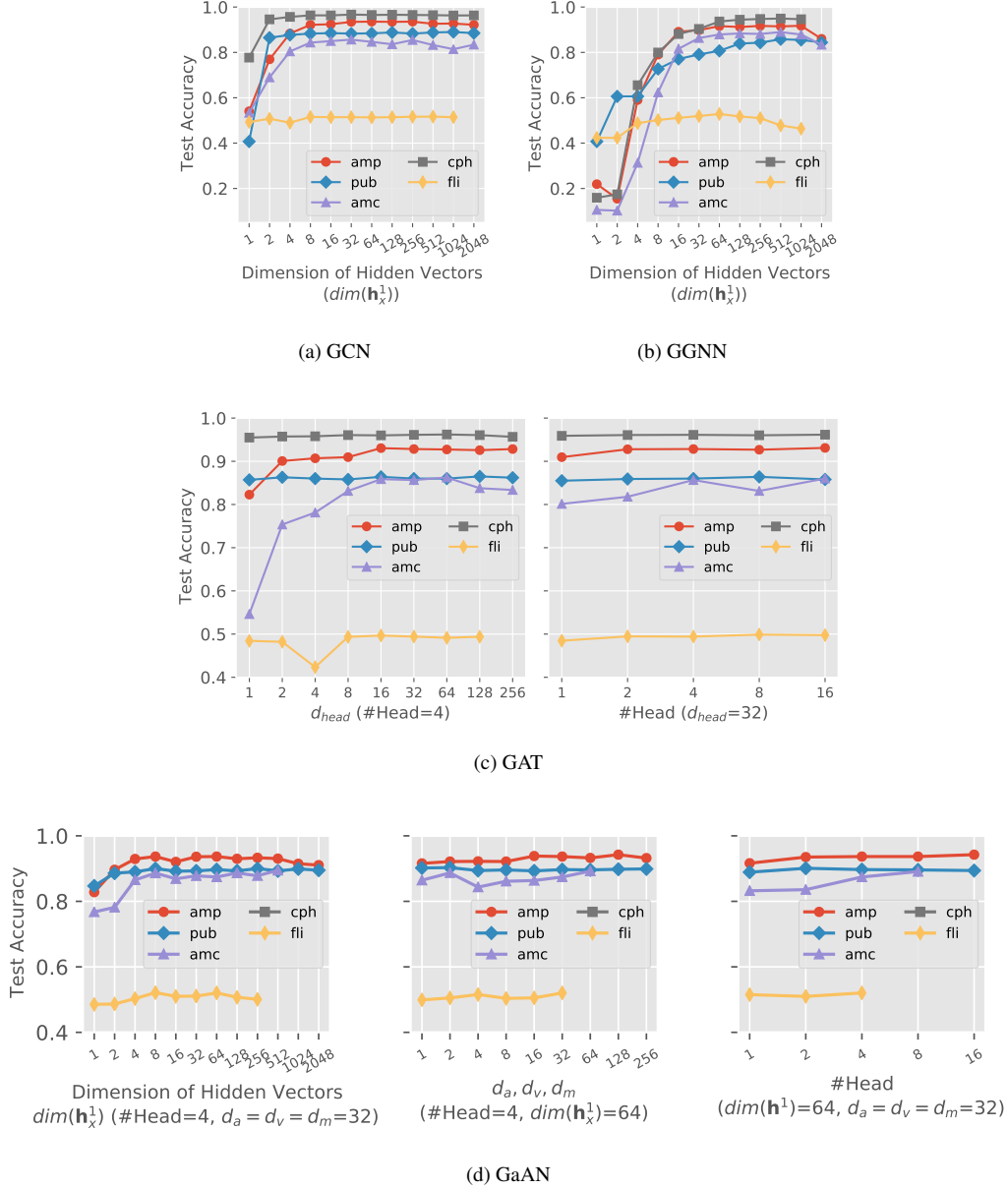
Figure 13: Effects of hyper-parameters on the accuracy of the typical GNNs.

Figure 14 further compares the best accuracy that every GNN achieved on different datasets. The best accuracy of the four GNNs was very close. It was also close to the accuracy reported in [33, 31]. The results indicated that there was no clear winner. The relative accuracy between GNNs varied greatly with different datasets. GaAN achieved the highest accuracy in three out of five datasets. GCN achieved the highest or second-highest accuracy in three out of five datasets, though its model was simplest. Simple GNN models (such as GCN) could still achieve good accuracy with proper hyper-parameter settings.
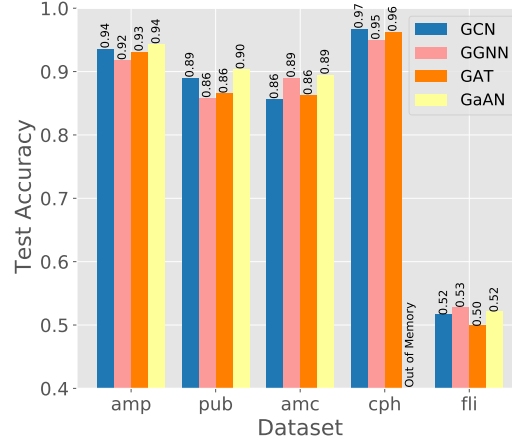
Figure 14: Best accuracy that each GNN achieved on different datasets.

Summary. The complexity analysis in Table 2 and Table 3 was valid for both training and inference. Fixing other hyper-parameters, each hyper-parameter itself affected the training/inference time and the memory usage of a GNN layer *in a linear way*. Algorithm engineers could adjust hyper-parameters according to the complexity analysis to avoid explosive growth in the training/inference time and memory usage. The accuracy of GNNs was much more sensitive to the dimension of hidden vectors/heads than the other hyper-parameters. The relative accuracy between GNNs varied greatly with different datasets. Simple GNN models (such as GCN) could achieve good accuracy with proper hyper-parameter settings.

4.2. Time Breakdown Analysis

To find out which stage/step dominated the training/inference time, we decomposed the training/inference time and analyzed performance bottlenecks level by level. We first analyzed the training time in Section 4.2.1 to Section 4.2.3. The similarities and differences between training and inference were analyzed in Section 4.2.4.

4.2.1. Layer Level

Figure 15 decomposes the training time of a GNN on the layer level. The training time of each layer was the summation of the time in the forward, backward, and evaluation phases. In GCN, GAT, and GaAN, the time spent on the layer 0 was much larger than the layer 1. In those GNNs, the dimensions of the input/output hidden vectors in the layer 0 were much larger than the dimensions in the layer 1: $d_{in}^0 = dim(\boldsymbol{v}_x)$, $d_{out}^0 = d_{in}^1 = 64$, $d_{out}^1 = \#Class$, and $dim(\boldsymbol{v}_x) \gg \#Class$. For GaAN, since it required the dimensions of the input/output hidden vectors must be the same, the hyper-parameters were set to $d_{in}^0 = d_{out}^0 = d_{in}^1 = d_{out}^1 = 64$ and the training time of both layers was close.
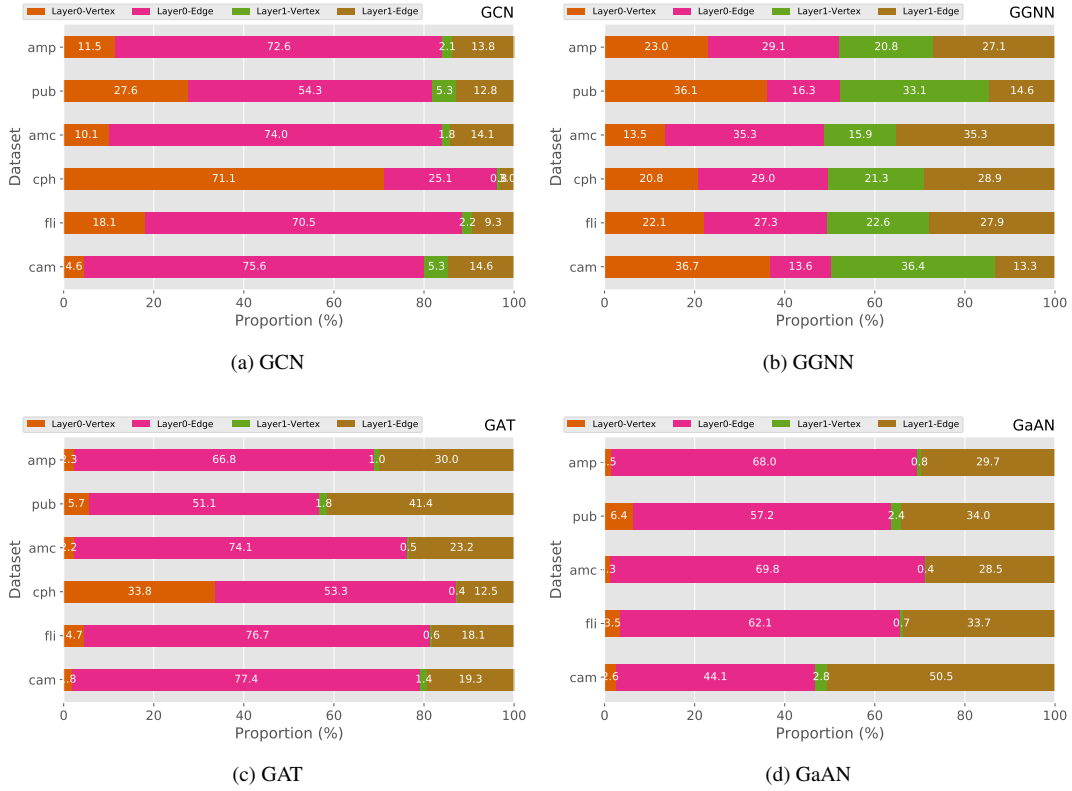
Figure 15: Training time breakdown on the layer level. The training time of each layer included the time spent on the forward, backward, and evaluation phases. Each layer was further decomposed into the vertex and the edge calculation stages.

Each GNN layer was further divided into the vertex and edge calculation stages. In Figure 15, GCN spent most of the training time on the edge calculation stage on most datasets. A special case was the cph dataset. The dimension of the input feature vectors was very high in cph, making the vertex calculation stage of the GCN Layer 0 spend considerable time. GGNN also spent the majority of its training time on the edge calculation stage, but the high time complexity of its vertex updating function γ^l made the proportion of the vertex calculation in the total training time much higher than the other GNNs. For GAT and GaAN, due to their high edge calculation complexity, the edge calculation stage was the dominant stage.

The experimental results also indicated that the average degree of the dataset affected the proportion of the edge/vertex calculation time in the total training time. For GaAN, the time spent on the vertex calculation stage exceeded the edge calculation stage on the pub and cam datasets, because the average degrees of the two datasets were low, making $|\mathcal{E}|$ and $|\mathcal{V}|$ much closer. To evaluate the effects of the average degree, we generated random graphs with 50,000 vertices and average degrees ranging from 2 to 100. Figure 16 shows the training time of the four GNNs under different average degrees. As the average degree increased, the training time of the edge calculation stage grew *linearly*. For GCN, GAT, and GaAN, the edge calculation stage dominated the entire training time even when the average degrees were small. Only for GGNN that had high vertex and low edge calculation complexity, the training time of the vertex calculation stage exceeded the edge calculation stage under low average degrees (< 5).

In summary, *the edge calculation stage was the most time-consuming stage in GNN training*. Improving its efficiency was the key to reduce the GNN training time.

(a) GCN

(b) GGNN

(c) GAT

(d) GaAN
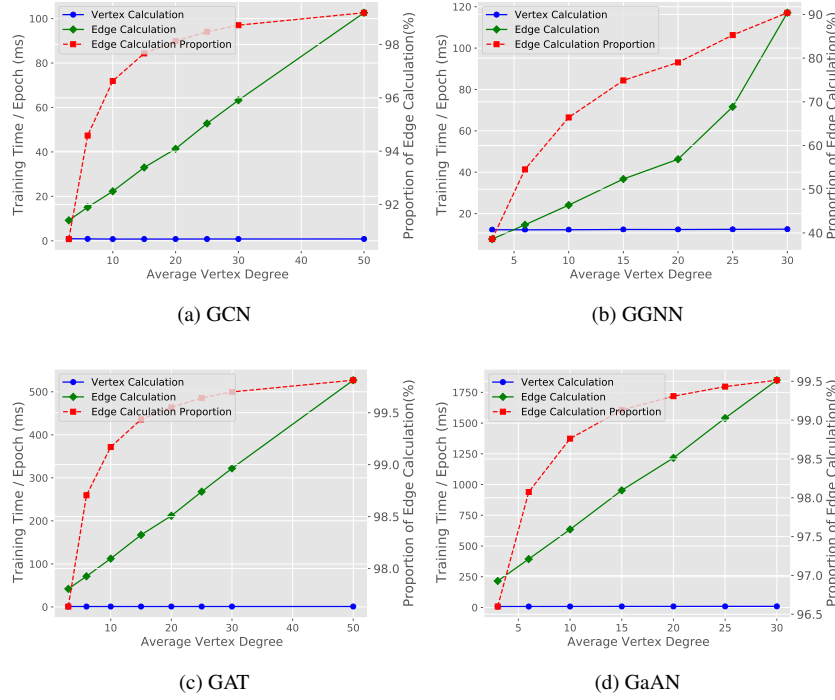
Figure 16: Effects of average degrees on the vertex/edge calculation time. Graphs were generated with the R-MAT generator by fixing the number of vertices as 50,000.

4.2.2. Step Level in Edge Calculation

We further investigated the most time-consuming step of the edge calculation stage. In the implementation of PyG, the edge calculation stage consisted of four steps: collection, messaging, aggregation, and vector updating, as shown in Figure 17. The edge index was a matrix with $|\mathcal{E}|$ rows and two columns. It held the edge set of the graph. The two columns of the edge index stored the source and the target vertex IDs of each edge.
465 The collection step copied the hidden vectors from the previous GNN layer $\boldsymbol{h}_y^l$ and $\boldsymbol{h}_x^l$ to the both endpoints of each edge $e_{y,x}$ in the edge index, forming the parameter tensor $[\boldsymbol{h}_y^l, \boldsymbol{h}_x^l, \boldsymbol{e}_{y,x}]$ of the messaging function ϕ^l. This step only involved data movement. The messaging step called the messaging function ϕ^l on all edges to get message vectors $\boldsymbol{m}_{y,x}^l$. The aggregation step aggregated the message vectors with the same target vertex
470 into an aggregated vector $\boldsymbol{s}_x^l$. The vector updating step was optional. It performed an additional transformation on the aggregated vectors (for example, adding the bias in GCN).
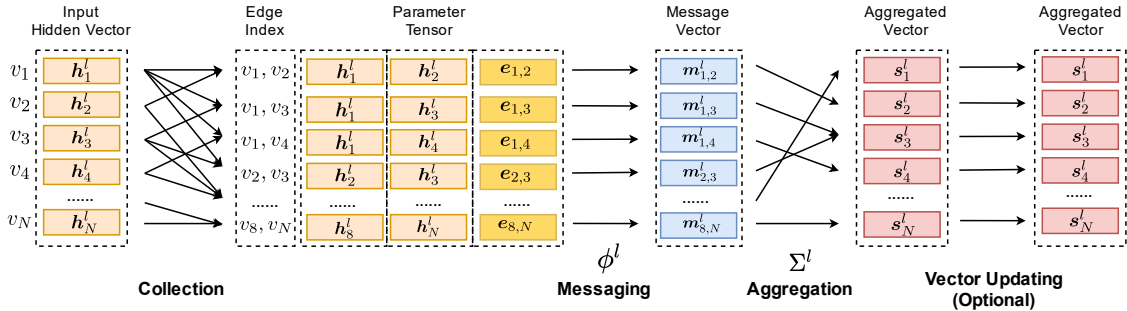
Figure 17: Step decomposition of the edge calculation stage of the GNN layer l.

We decomposed the execution time of the edge calculation stage in Figure 18. In each GNN, the proportions of the four steps were rather stable, rarely affected by datasets. For GAT and GaAN with the high edge calculation complexity, the messaging step consumed most of the training time. For GCN and GGNN with the low

edge complexity, the proportions of the steps were close. Since the messaging function ϕ^l of GGNN used the pre-computed $\hat{\boldsymbol{h}}_y^l$ as the message vector directly, the time spent on the messaging step of GGNN was negligible. Although the collecting step did not conduct any computation and only involved data movement, it occupied a noticeable execution time in the four GNNs.

The results indicate that *the performance bottlenecks of the edge calculation stage depend on the complexity of the messaging function ϕ.* When the time complexity of ϕ was high, the messaging step was the performance bottleneck. Optimizing the implementation of ϕ could significantly reduce training time. Otherwise, the collection and the aggregation steps were performance bottlenecks. Improving the efficiency of the two steps could benefit all GNNs.
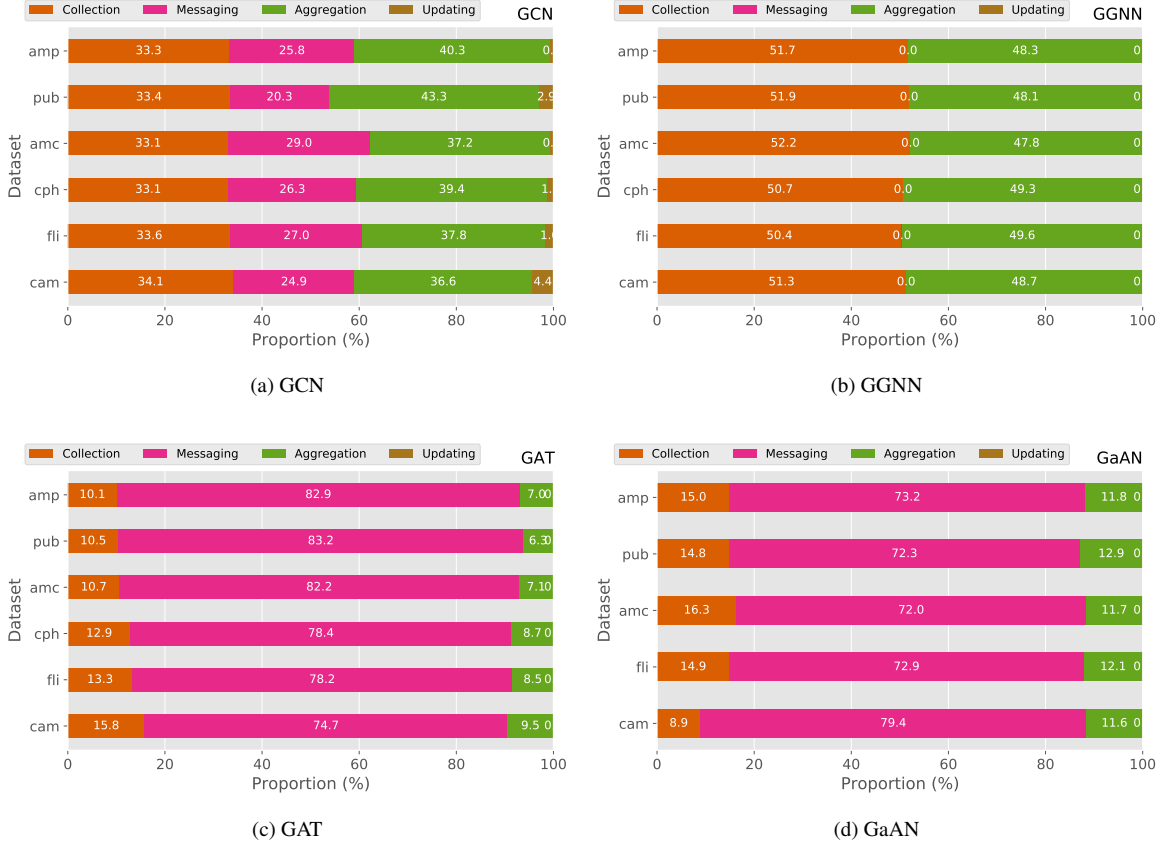
Figure 18: Training time breakdown of the edge calculation stage.

4.2.3. Operator Level

The functions ϕ, Σ and γ in the edge and vertex calculation stages were made up of a series of basic operators implemented on the GPU side, such as the matrix multiplication `mm`, the elementwise multiplication `mul` and the index-based selection `index_select`. Figure 19 shows the top-5 time-consuming basic operators of training each GNN, averaged over all datasets.
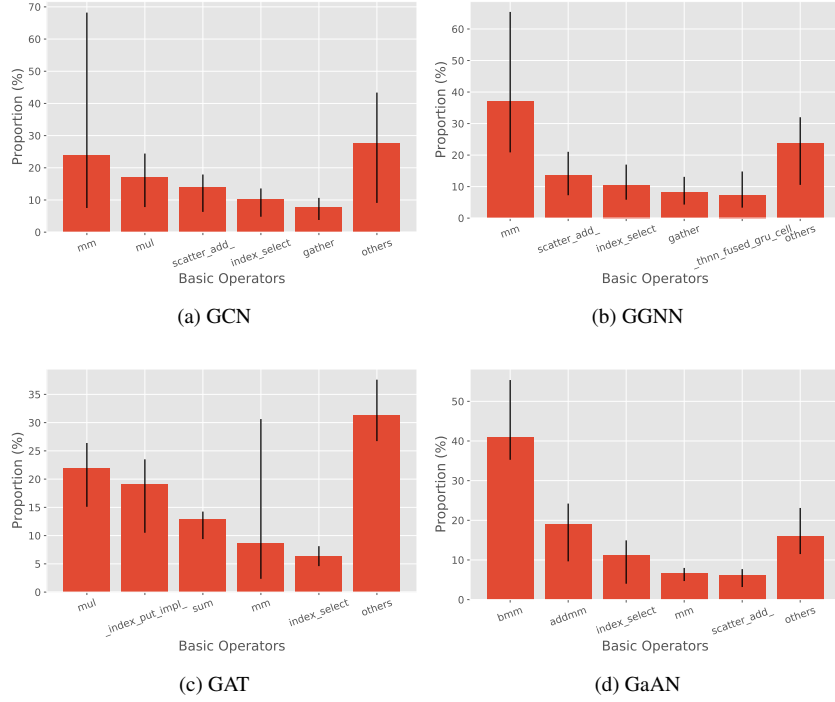
Figure 19: Top 5 time-consuming basic operators in training. The time proportion of each basic operator was averaged over all datasets with the error bar indicating the maximum and the minimum.

GCN. The most time-consuming basic operator was the matrix multiplication mm used in the vertex updating function γ. The elementwise multiplication mul used in the messaging function ϕ was also time-consuming. The other three operators were used in the edge calculation stage: scatter_add_ for the aggregation step in the forward phase, gather for the aggregation step in the backward phase, and index_select for the collection step. For GCN, the basic operators related to the edge calculation stage consumed the majority of the training time.

GGNN. The top basic operator was mm used in the vertex updating function γ. Due to its high time complexity, the proportion of mm was much higher than the other operators. The thnn_fused_gru_cell operator was used in both the forward and backward phases of γ. The other three operators were used in the edge calculation stage.

GAT. All the top basic operators except for mm were related to the edge calculation stage. The mm operator was used in the vertex updating function γ.

GaAN. The top basic operator was bmm used in the messaging function ϕ. The addmm operator and the mm operator were used in both the vertex and the edge calculation stages, where the edge calculation stage was dominant.

The most time-consuming operators in the four GNNs were the matrix multiplication mm and the elementwise multiplication mul, *making GNN training suitable for GPUs*. Although the aggregation step in the edge calculation stage was relatively simple (like sum and mean), the related operators–scatter_add and gather–still consumed a certain amount of the time. The two operators had to synchronize between hardware threads to avoid updating the same aggregated vector at the same time. They also conducted non-regular memory access with the access pattern determined by the edge set dynamically. For GPUs, they were less efficient than mm. The index-based selection operator index_select used in the collection step consumed about 10% of the training time in all GNNs. Improving the efficiency of scatter_add/gather/index_select could benefit all kinds of GNNs.

4.2.4. *Comparing Inference and Training*

We found that the performance characteristics of GNN inference were highly similar to training on the *layer* level and the *step* level. Taking GCN as an example, Figure 20 shows the time breakdowns of GCN inference on the *layer* level and *step* level of the edge calculation. By cross-comparing Figure 15a with Figure 20a, Figure 16a with Figure 20b, and Figure 18a with Figure 20c, the time breakdowns of training and inference were very similar. For the other GNNs, we observed similar phenomena.

(a) Layer level

(b) Effects of average degrees

(c) Step level of the edge calculation stage
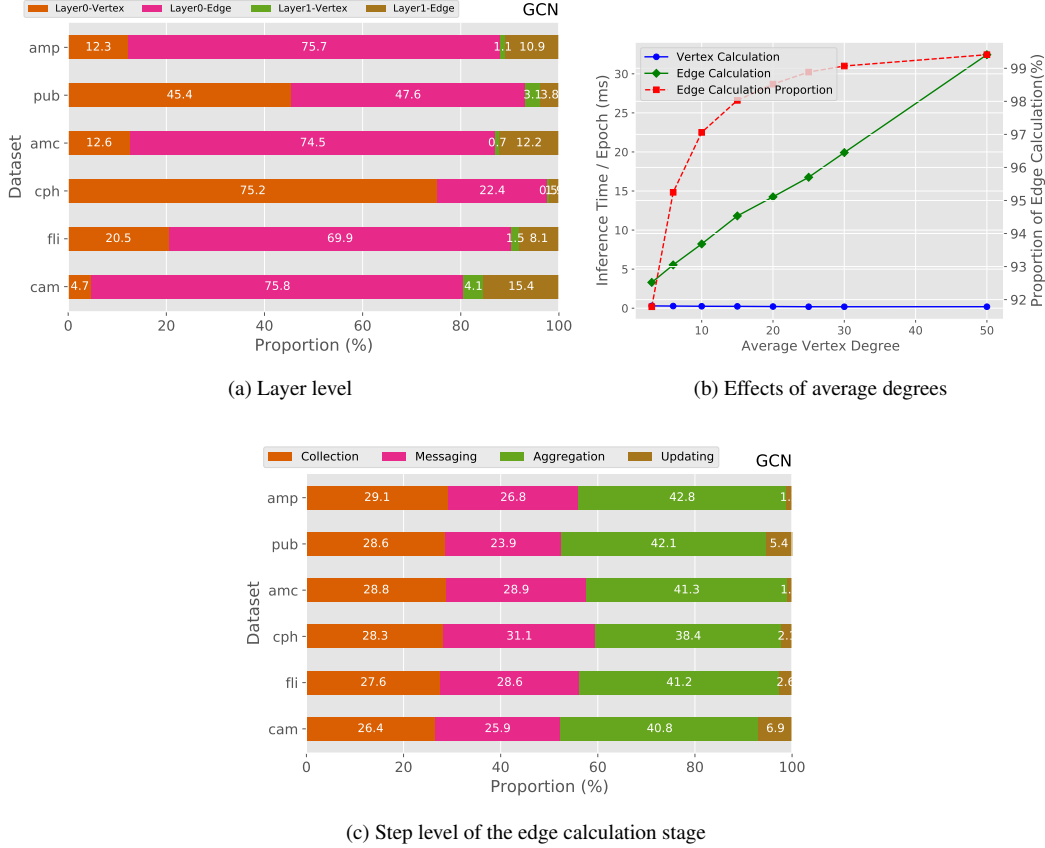
Figure 20: Time breakdowns of GCN inference.

The main differences between training and inference were reflected in two aspects: the wall-clock time and the top time-consuming basic operators. The inference time was much less than the training time. Figure 21 compares the wall-clock time of training and inference on the amp, amc, and fli datasets. The results on the other datasets were similar. Since the inference only conducted the forward propagation from the input layer to the prediction layer, the inference time was very close to the time of the forward phase in training. The inference time was 34% (GCN), 32% (GGNN), 25% (GAT), and 32% (GaAN) of the training time, averaged over all datasets.
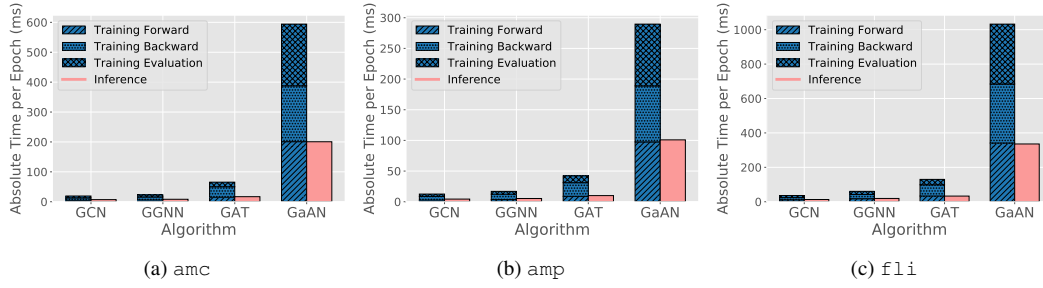
Figure 21: Wall-clock inference time on different datasets.

The top time-consuming basic operators of training and inference also showed a certain degree of difference. Some of the top time-consuming operators during training were replaced by new operators in inference. Figure 22 shows the top 5 time-consuming basic operators in inference. For GCN, the `index` operator used in the prediction layer became the new top 5 time-consuming operators, replacing the `gather` operator used in the backward phase in training. For GGNN, `index` operator in the prediction layer also became a time-consuming basic operator. For GAT, the `input_put_impl` operator (used in the backward phase) in Figure 19c was replaced by the `scatter_add` operator used in the forward edge calculation in Figure 22c. For GaAN, the `mm` operator was replaced by the `cat` operator used in the vertex updating function.

Although some specific time-consuming operators were different, the performance bottlenecks on the operator level were the same for training and inference. The matrix multiplication `mm` and the element-wise multiplication `mul` operators were still time-consuming for inference, making GNN inference also suitable for GPUs. The basic operators related to the collection and aggregation steps in the edge calculation still consumed non-trivial time in inference.
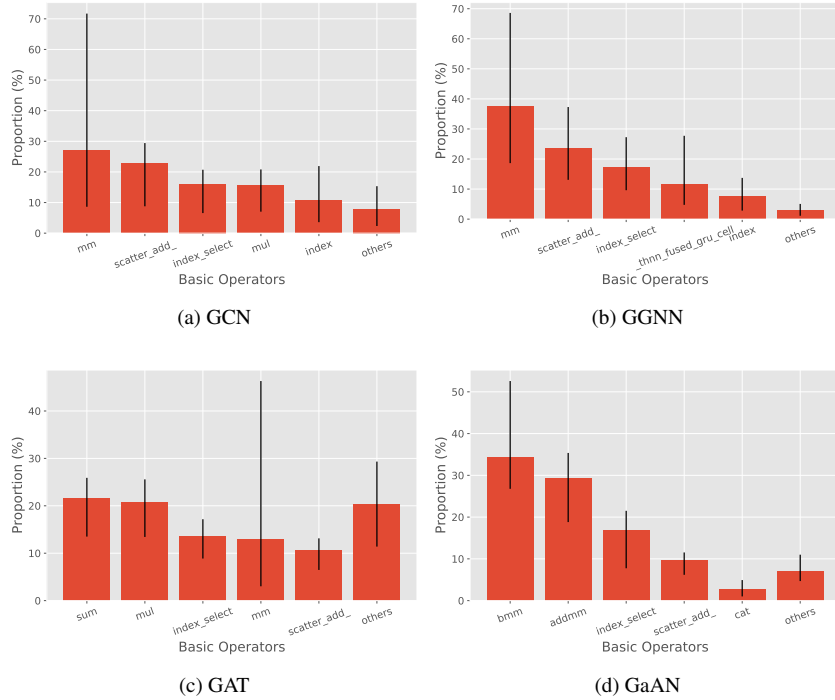
Figure 22: Top 5 time-consuming basic operators in inference. The time proportion of each basic operator was averaged over all datasets with the error bar indicating the maximum and the minimum.

Summary of Time Breakdown Analysis. The GNN training/inference was suitable for GPUs. The edge calcu-
lation stage was the main performance bottleneck in most cases, except for processing GNNs with high vertex
calculation complexity on low-average-degree graphs. The performance bottlenecks in the edge calculation
stage depended on the time complexity of the messaging function ϕ. If the time complexity of ϕ was high, ϕ
dominated the training/inference time of the edge calculation stage. Optimizations should focus on improving
its efficiency. Otherwise, the collection step and the aggregation step dominated the training/inference time. The
collection step suffered from lots of data movement. The aggregation step suffered from data synchronization
and non-regular data access.

4.3. Memory Usage Analysis

Training. During the GNN training, we stored all data (including datasets and intermediate results) in the on-
chip memory of the GPU. Compared with the main memory on the host side (90 GB), the capacity of the GPU
memory (16 GB) was very limited. *The GPU memory capacity limited the scales of the graphs that it could
handle.* For example, GaAN was unable to train on the `cph` dataset due to the out of memory exception.

Figure 23 shows the peak memory usage of each phase during the GNN training on the `amp` dataset. The
trends on the other datasets were similar. *The GNN training achieved its peak memory usage in the forward
and the backward phases.* The forward phase generated lots of intermediate results. Some key intermediate
results were cached for the gradient calculation in the backward phase, increasing memory usage. For example,
Figure 24 shows the computation graph of the vertex updating function γ^l of GGNN. Each operator in the
computation graph generated an intermediate tensor. Some key intermediate tensors were cached. The cached
tensors were the main source of memory usage in the loss phase. By the end of the backward phase, the
cached tensors were released. Since the evaluation phase did not have to calculate the gradients, it did not cache
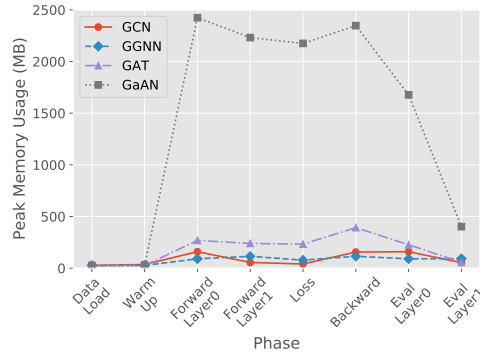intermediate tensors. Its memory usage declined sharply.

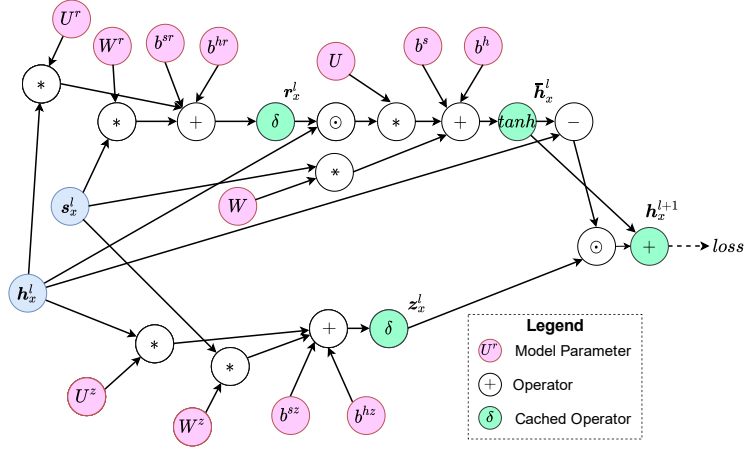Figure 23: Memory usage of each phase during the GNN training. Dataset: `amp`.

Figure 24: Computation graph of the vertex updating function γ of GGNN.

The peak memory usage during the GNN training far exceeded the size of the dataset itself. We defined the *memory expansion ratio* (MER) as the ratio of the peak memory usage during the training to the memory usage after loading the dataset. Figure 25 compares MER of different GNNs. GCN had the lowest MER (up to 15.2) while GaAN had the highest MER (up to 104.6). *The high MERs limited the data scalability of GNNs*, making GPUs unable to handle big graphs. Figure 25 also indicates that the same GNN had different MERs for different datasets. Two characteristics of a dataset affected the MER: the dimension of the input feature vectors and the average degree of the graph.
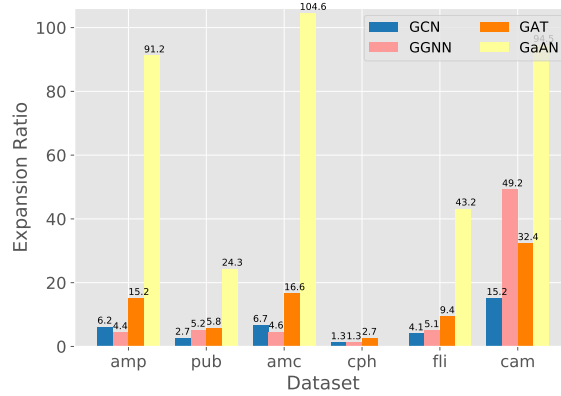
Figure 25: Memory expansion ratios of typical GNNs.

To find out how the dimension of input feature vectors affected the MER, we generated random input feature vectors with different dimensions for the `cam` dataset and measured the MER in Figure 26. Under the same hyper-parameters, *the MER decreased as the dimension of input feature vectors increased*. When the dimension of the input feature vectors was high, the size of the dataset itself was large. The size became comparable to the size of intermediate results, making MERs low.
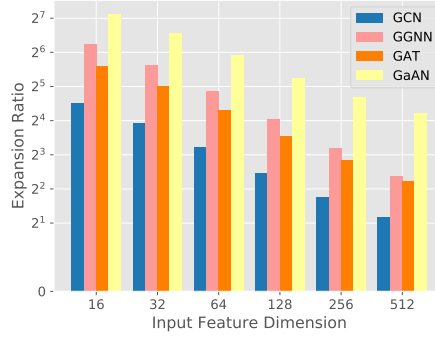
Figure 26: Memory expansion ratio under different dimensions of input feature vectors. Dataset: `cam`.

Average degrees also affected MERs by influencing the relative sizes of intermediate results from the edge and the vertex calculation stages. Fixing the number of vertices $|\mathcal{V}|$, we generated random graphs with different average degrees. Figure 27 shows how the memory usage changed according to the average degree. As the average degree $\bar{d}$ increased, the peak memory usage increased *linearly* with $\bar{d}$. The edge calculation stage gradually dominated the memory usage and *the MER converged to a stable value*. The stable value was determined by the complexity of the edge calculation stage. Except for GGNN, the MERs of the other GNNs increased as $\bar{d}$ increased. As GGNN had high vertex calculation complexity, the MERs related to the vertex calculation stage were much higher than the edge calculation stage. When the edge calculation stage dominated the memory usage, its MERs became smaller.

(a) Peak memory usage

(b) Memory expansion ratio
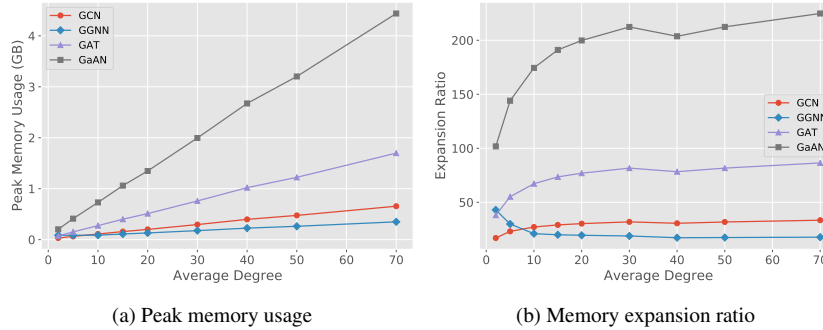
Figure 27: Memory usage under different average degrees. The random graphs were generated by fixing the number of vertices at 10K and the dimension of input feature vectors at 32.

We also fixed the number of edges $|\mathcal{E}|$ and generated random graphs with different $|\mathcal{V}|$. Figure 28 shows how the memory usage changed according to $|\mathcal{V}|$. MERs of all GNNs were insensitive to $|\mathcal{V}|$, compared to $|\mathcal{E}|$. Except for GGNN, the MERs of the other GNNs declined as $|\mathcal{V}|$ increased because the sizes of the datasets increased more quickly than the sizes of the intermediate results. As GGNN had high vertex calculation complexity, the sizes of the intermediate results were very sensitive to $|\mathcal{V}|$. It indicated that *the intermediate results of the edge calculation stage dominated the memory usage during the GNN training*.

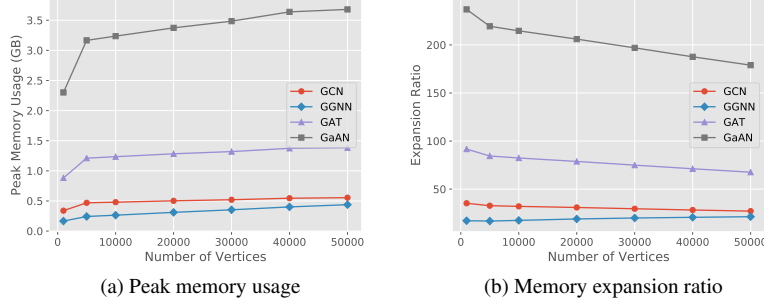28

(a) Peak memory usage

(b) Memory expansion ratio

Figure 28: Memory usage under different numbers of vertices. The random graphs were generated by fixing the number of edges at 500K and the dimension of input feature vectors at 32.

Inference. Figure 29 shows the memory expansion ratios of typical GNNs during inference. Since no intermediate results had to be cached during inference of GGNN, GAT, and GaAN, the MERs of inference were much less than training for the three GNNs (compared with Figure 25). The MERs of inference were 45% to 83% (GGNN), 52% to 61% (GAT), and 37% to 69% (GaAN) of training. However, the MERs were still high, disallowing inferencing with big graphs. To handle big graphs, the sample-based inference was necessary.
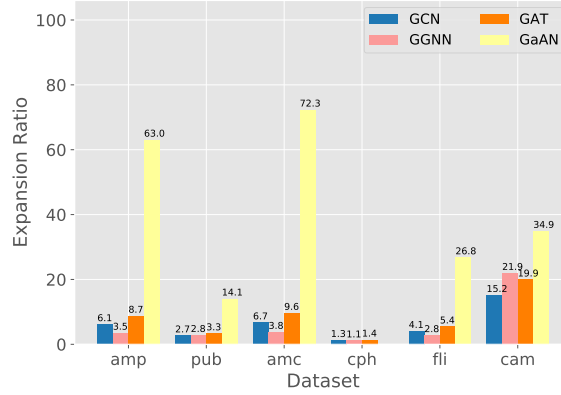
Figure 29: Memory expansion ratios of typical GNNs in Inference.

We also conducted experiments about the effects of input feature dimensions, average degrees, and the number of vertices on the memory usage of inference. The results were similar to GNN training.

Summary of Memory Usage Analysis. The *high* memory expansion ratio severely restricted the data scalability of GNN training and inference. The memory usage mainly came from the intermediate results of the *edge calculation stage*. Fixing the number of vertices, the memory usage increased *linearly* along with the number of edges. Fixing the GNN structure and the hyper-parameters, increasing the dimension of input feature vectors could reduce the memory expansion ratio. To reduce the memory usage of GNN training and inference, optimizations should focus on reducing memory footprints of the edge calculation stage.

4.4. Effects of Sampling Techniques on Performance

With the sampling techniques, GNNs were trained and performed inference in a mini-batch manner. Each epoch was decomposed into many batches. In each batch, PyG only sent the sampled subgraph to the GPU to train or inference. The batch size determined the size of the sampled subgraph. Thus, it affected the accuracy, training/inference time, and memory usage simultaneously.

4.4.1. Size of Sampled Subgraphs

Figure 30 shows how the size of the sampled subgraph changed with the batch size. For the neighbor sampler, the relative batch size was defined as the proportion of the sampled vertices of the last GNN layer in $\mathcal{V}$. For the cluster sampler, the relative batch size was defined as the proportion of the sampled partitions in all partitions of the graph. The experimental results indicated that the neighbor sampler was very sensitive to the batch size. As the batch size increased, the size of the sampled subgraph first increased quickly and then stabilized. The cluster sampler was much less sensitive compared to the neighbor sampler. The number of vertices and the average degree of the sampled subgraphs increased linearly with the batch size.

(a) Neighbor sampler

(b) Cluster sampler
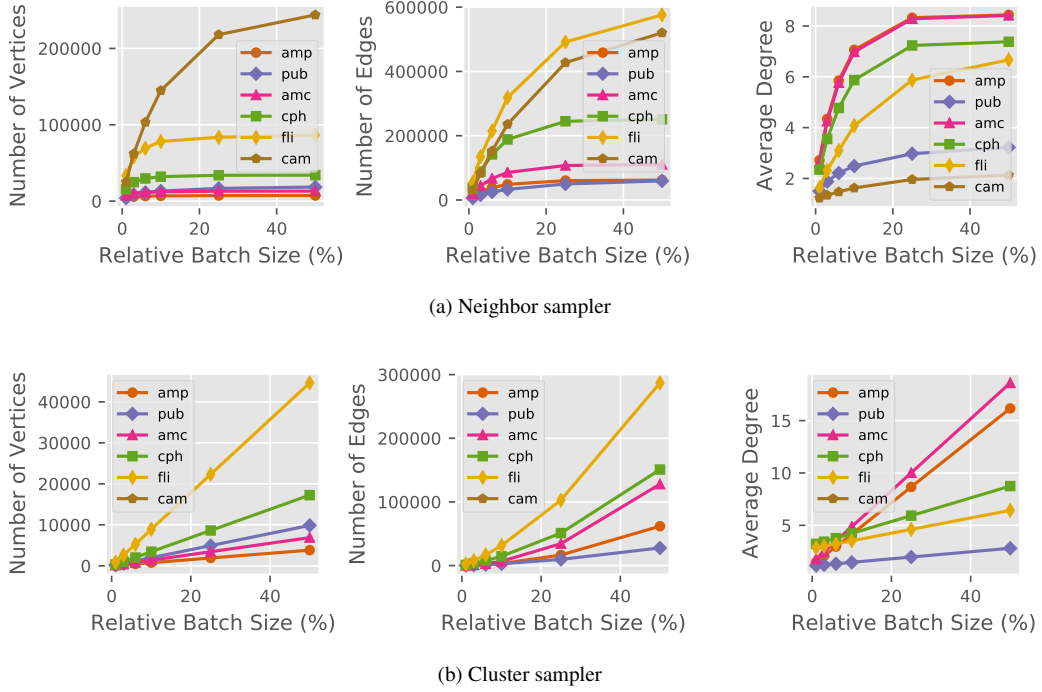
Figure 30: Sizes of sampled subgraphs under different relative batch sizes. The batch size was relative to the full graph. Each batch size was sampled 50 times and the average values were reported. The error bar indicates the standard deviation.

The average degree of the sampled subgraph was *much lower* than the average degree of the original graph, especially when the relative batch size was low. Taking the neighbor sampler with the relative batch size of 6% as an example, the average degree of the amp dataset was 31.1, but the average degree of the sampled subgraph was only 5.8. For the cluster sampler, the average degree was 3.0. Figure 31 compares the degree distribution of the sampled subgraphs with the original graph. The slopes of the curves were similar, indicating that the sampled subgraphs still followed the power-law degree distribution. However, the numbers of high-degree vertices were much less than the original graph, lowering the average degrees. According to the experimental results in Section 4.2, if the average degree became lower, the proportion of the training time spent on the vertex calculation stage would become higher, especially for GGNN.
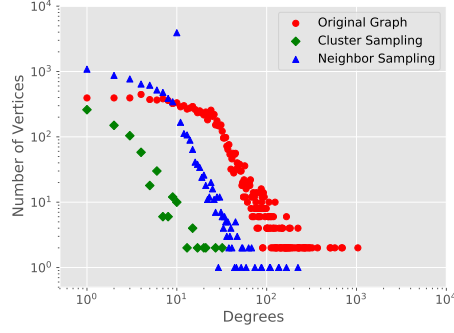
Figure 31: Vertex degree distribution of the sampled subgraph (relative batch size: 6%) and the original graph. Dataset:`amp`.

4.4.2. Performance Bottlenecks in Sample-based Training

To find out performance bottlenecks of the sampling techniques, we decomposed the training/inference time per batch into three phases: *sampling* on the CPU side, *transferring* sampled subgraphs from the CPU side to the GPU side, and *training/inference* with the sampled subgraphs on the GPU side.
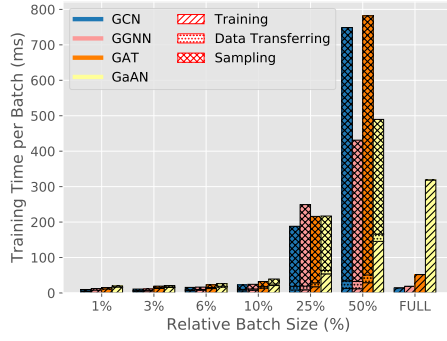
Figure 32 shows the *training* time breakdown of the four GNNs under different relative batch sizes. For the neighbor sampler, the sampling technique reduced the training time per batch only when the batch size was very small. When the batch became bigger, the sampling and the data transferring phases introduced noticeable overheads, making the training time exceed the full-batch training. For the clustering sampler, the sampled subgraph was smaller than the neighbor sampler under the same relative batch size. The reduction in the training time was more obvious than the neighbor sampler. However, the overheads increased quickly as the relative batch size increased. The training time under the 25% relative batch size already exceeded the time of full-batch training. The experimental results indicated that the current implementation of the sampling techniques in PyG was inefficient. When the batch size was large, more than 50% of the time had been spent on sampling and data transferring. *The sampling techniques were only efficient under small batch sizes.*
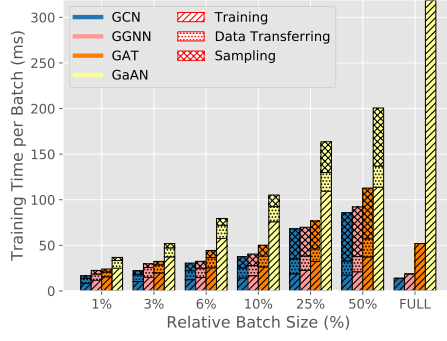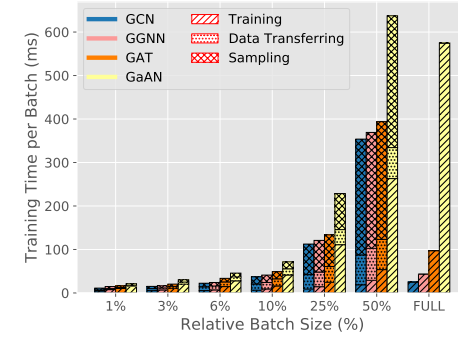
31

(a) Neighbor sampler on `amc`
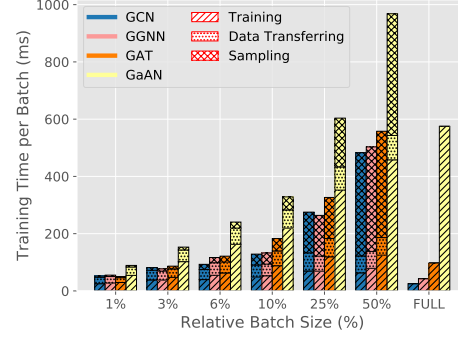
(b) Neighbor sampler on `fli`

(c) Cluster sampler on `amc`

(d) Cluster sampler on `fli`

Figure 32: Training time per batch breakdown. FULL means that the full graph participates in the training.

The main advantage of the sampling techniques was *reducing the peak memory usage* during training. Figure 33 shows the memory usage under different batch sizes. The peak memory usage declined significantly even under big batch sizes. The sampling techniques made training GNNs on big graphs *possible* for GPUs.
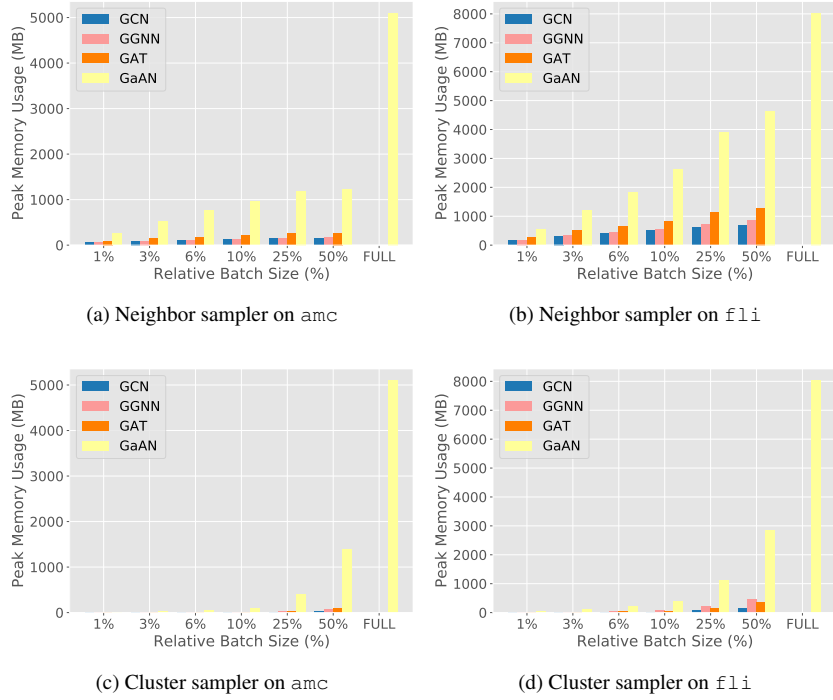
(a) Neighbor sampler on `amc`

(b) Neighbor sampler on `fli`

(c) Cluster sampler on `amc`

(d) Cluster sampler on `fli`

Figure 33: Peak memory usage under different batch sizes. FULL means that the full graph participated in the training.

The disadvantage of the sampling technique was wasting GPU resources. As the sampling techniques were only effective under small batch sizes, the sampled subgraphs were very small in those cases. They could not make full use of the computing power of a GPU. To simulate the situation, we generated random graphs with few vertices and measured their training time per epoch in Figure 34. As the number of vertices increased, the training time was almost unchanged except for GaAN. The training time of GaAN increased only when $|\mathcal{V}| \geq 4000$.
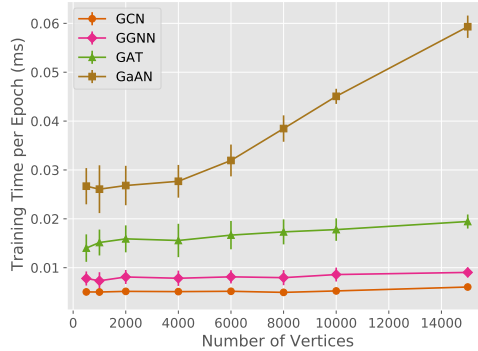

Figure 34: Training time per epoch on small random graphs. For each number of vertices, we generated 50 random graphs with an average degree of 4.0 and reported the average training time per batch (without the evaluation phase). The error bar indicates the standard deviation.

4.4.3. Performance Bottlenecks in Inference

The sample-based inference was an effective technique to conduct inference on big graphs. Taking the node classification task as an example, to predict labels for a given set of vertices $\mathcal{V}_{predict}$, the inference sampler sampled a subgraph containing complete L-hop neighborhoods of all vertices in $\mathcal{V}_{predict}$, where L was the number of GNN layers. Since the real-world graphs often had small-world property, the size of the sampled subgraph increased quickly as the number of vertices in $\mathcal{V}_{predict}$ (i.e., batch size) increased. Figure 35 shows how the

relative batch size ($\frac{|\mathcal{V}_{predict}|}{|\mathcal{V}|}$) affected the average degree and the number of edges of the sampled subgraphs during inference. When the relative batch size was 10%, the number of edges in the sampled subgraphs were close to the number of edges in the whole graph in most datasets. To limit the memory usage during inference, the batch size used should be very small in inference.
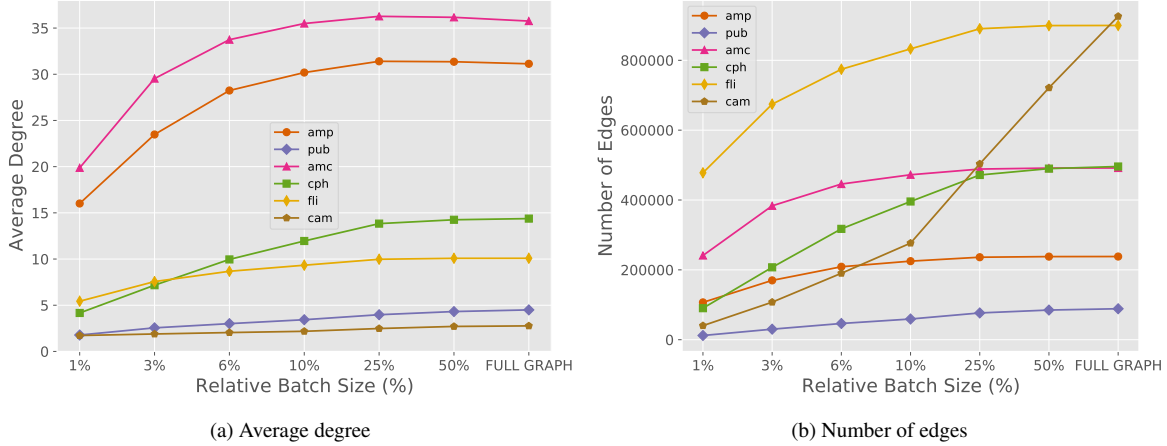

(a) Average degree

(b) Number of edges

Figure 35: Sizes of sampled subgraphs produced by the inference sampler under different relative batch sizes.

However, the overheads brought by sampling and data transferring from CPU to GPU became obvious when the batch size was small. Figure 36 shows the time breakdowns of sample-based inference on different datasets. The On the amp and cam datasets, the sampling time even accounted for near half of the total inference time. The results indicated that the current implementation of inference sampler in PyG was also inefficient. Improving its efficiency could significantly reduce the sample-based inference time.
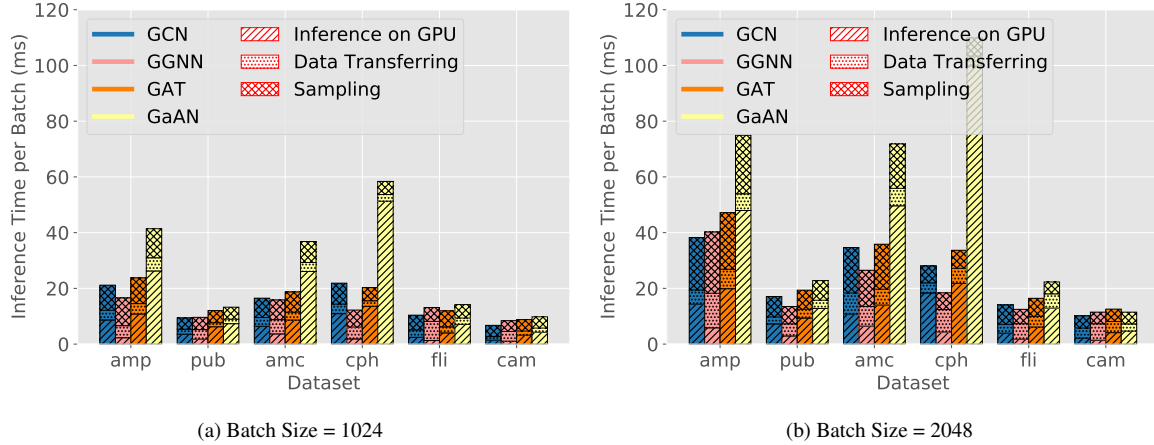

(a) Batch Size = 1024

(b) Batch Size = 2048

Figure 36: Inference time per batch breakdown under different batch sizes.

4.4.4. Effects on Accuracy

Since the size of the sampled subgraph was much smaller than the original graph, the accuracy of the GNN models trained with sampling techniques might be different from the full-batch training. To find out how the batch size affected the test accuracy, we trained GNNs with different batch sizes. Figure 37 and Figure 38 compare the test accuracy achieved by sampling techniques with the test accuracy of the full-batch training. For each combination of dataset and GNN, we chose the hyper-parameters that achieved the highest accuracy according to the experimental results in Section 4.1.4.
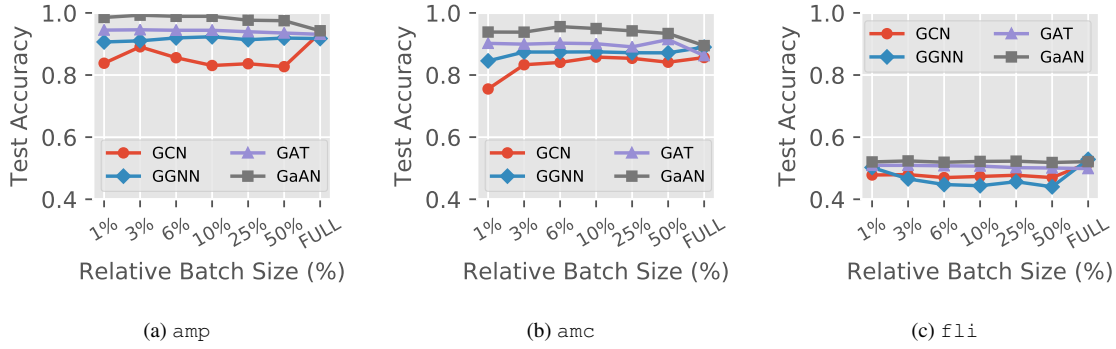
(a) `amp` (b) `amc` (c) `fli`

Figure 37: Test accuracy under different batch sizes of the neighbor sampler. FULL means that the full graph participated in the training.
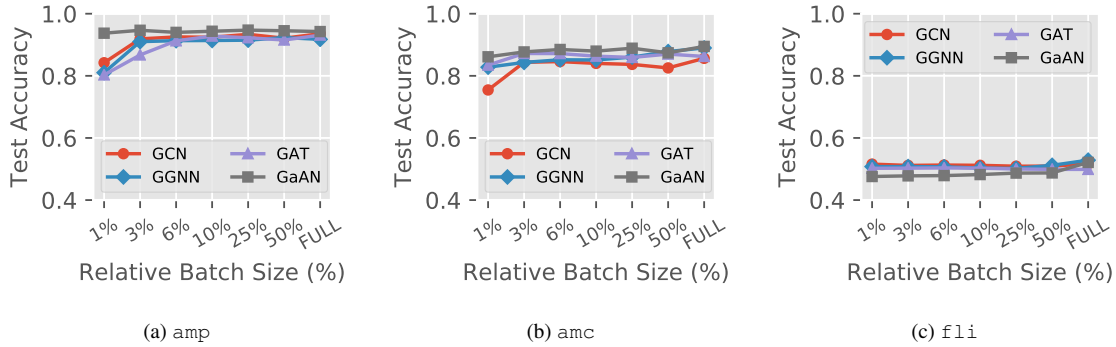

(a) `amp` (b) `amc` (c) `fli`

Figure 38: Test accuracy under different batch sizes of the cluster sampler. FULL means that the full graph participated in the training.

The experimental results confirmed the effectiveness of the sampling methods in terms of accuracy. When the relative batch size was greater than or equal to 3%, the test accuracy of the GNNs trained with sampling was close to the accuracy obtained by full-batch training. In most cases, the accuracy achieved by the sampling techniques was slightly lower than the full-batch training. However, there were some exceptions (like GaAN in Figure 38a and Figure 38b) that the accuracy achieved by sampling was even higher.

The relationships between batch size and test accuracy were complex. A larger batch size did not always bring higher accuracy. For example, the accuracy of GaAN in Figure 38a and GGNN in Figure 38c decreased as the batch size increased. A smaller batch size sometimes could achieve higher accuracy. For example, GAT achieved a higher accuracy with 1% relative batch size than the full-batch training in Figure 38b. Given a sampling method, we found that the optimal batch size highly depended on the dataset and the GNN algorithm. Our observations were similar to [31]. How to automatically select a proper batch size is a topic worth further studying.

Among the two sampling methods, the performance of the cluster sampler was more stable than the neighbor sampler. With the cluster sampler, the test accuracy of different GNNs was very close to the accuracy of full-batch training. With the neighbor sampler, the test accuracy of different GNNs showed more obvious differences.

Summary of Sampling Techniques. The sampled subgraphs produced by the neighbor sampler and the cluster sampler had lower average degrees than the original graph. With small batch sizes, the sampling techniques could significantly reduce the peak memory usage per batch. However, the current implementation of the sampling techniques in PyG was inefficient to handle small batches. The time spent on the sampling phase and the data transferring phase could even exceed the training/inference phase. Small batches could not make full use of the computing power of a GPU either.

5. Insights

Through the extensive experiments, we propose the following key findings and suggestions for how to optimize the performance for GNN training and inference.

1. *The time complexity in Table 2 and Table 3 points out performance bottlenecks theoretically.* The experimental results validate the time complexity analysis. The time complexity points out where the bottleneck comes from. Optimization should focus on complex operations in the messaging function ϕ and the vertex updating function γ.

2. *The computational cost of a GNN layer is mainly affected by the dimensions of the input and output hidden vectors.* Theoretically and empirically, the training and inference time and the memory usage of a GNN layer both increase *linearly* with the dimensions of the input/output hidden vectors separately. GNNs are friendly to high-dimensional scenarios. Algorithm engineers can use high-dimensional feature vectors to improve the expressive power of a GNN without worrying about exponential growth in the training/inference time and memory usage

3. *Performance optimizations should focus on improving the efficiency of the edge calculation stage.* The edge calculation stage is the most time-consuming stage in most GNNs.

   - If the complexity of the messaging function ϕ is high, the implementation of ϕ is critical to performance. Improving its efficiency can significantly reduce training/inference time. For example, the attention mechanism in GNNs (like GAT and GaAN) requires an extra sub-layer to calculate the attention weight of each edge. Implementing the attention mechanism with specially optimized basic operators on the GPU side is a potential optimization direction.

   - If the complexity of ϕ is low, the efficiency of the collection step and the aggregation step becomes critical. The existing GNN libraries [15, 14, 16] already introduce the *fused* operator to improve their efficiency. When the messaging function ϕ is an assignment or a scalar multiplication of the input hidden vector of the source vertex, the libraries replace the collection, messaging, and aggregation steps with a single fused operator. The fused operator calculates the aggregated vectors directly from the input hidden vectors, minimizing the memory footprints and overlapping the memory accessing with computation. In this way, it significantly reduces the training/inference time of GNNs with low edge calculation complexity (like GCN) [19, 20]. However, the applicable condition of the fused operator is very restricted. It does not work for ϕ with more complex operations like matrix multiplication. A potential optimization is to develop composite CUDA kernels that can read the input hidden vectors and aggregate message vectors on the fly, without materializing the parameter vectors and the message vectors.

4. *The high memory usage caused by the intermediate results of the edge calculation stage limits the data scalability of GNN training/inference.* The memory expansion ratios of the typical GNNs are very high, making GPUs unable to handle big graphs. One solution is to distribute the dataset among several GPUs and frequently swap parts of the dataset between GPUs and the main memory [16]. Another possible solution [38] comes from the deep neural network training. It only checkpoints key intermediate results during the forward propagation and re-calculates the missing results on demand during the backpropagation. Implementing the checkpoint mechanism is another potential optimization for GNN training.

5. *Sampling techniques can significantly reduce the memory usage per batch, but its implementation is still inefficient.* The sampling techniques are effective under small batch sizes for both training and inference. The accuracy of the GNN models trained with the sampling techniques is close to the accuracy of full-batch training. With proper batch sizes, the accuracy of the sample-based training can be close to the accuracy of the full-batch training. However, the current implementation of the sampling techniques in PyG brings considerable overheads when the batch size is small. Improving the efficiency of the sampling techniques is a potential optimization direction. The small sampled subgraphs cannot make full use of the computing power of the GPU either. How to improve the GPU utilization under small batch sizes is another problem to solve. One possible solution is to train multiple batches asynchronously on the same GPU and use the asynchronous stochastic gradient descent to speed up the converge.

6. Related Work

Survey of GNNs. Zhou et al.[8], Zhang et al.[9] and Wu et al.[10] survey the existing graph neural networks and classify them from an algorithmic view. They summarize the similarities and differences between the architectures of different GNNs. The typical applications of GNNs are also briefly introduced. Those surveys focus on comparing the existing GNNs theoretically, not empirically.

Evaluation of GNNs. Shchur et al. [33] evaluate the accuracy of popular GNNs on the node classification task. Dwived et al. [39] further compare the accuracy of popular GNNs fairly in a controlled environment. Hu et al. [40] propose the open graph benchmark that provides standard datasets and a standard evaluation workflow. The benchmark makes comparisons between GNNs easily and fairly. Those model evaluation efforts focus on evaluating the accuracy of different GNNs. They provide insightful suggestions to improve accuracy.

From the efficiency aspect, Yan et al. [19] compare the performance characteristics of graph convolutional networks, typical graph processing kernels(like PageRank), and the MLP-based neural networks on GPUs. They provide optimization guidelines for both the software and the hardware developers. Zhang et al. [20] analyze the architectural characteristics of the GNN inference on GPUs under SAGA-NN [16] model. They find that the GNN inference has no fixed performance bottleneck and all components deserve to optimize. These two efforts focus on the *inference* phase of GNNs and they investigate the potential optimizations mainly from an architectural view. In this work, our target is to find out the performance bottleneck in the training phase from a system view. We consider the performance bottleneck in both time and memory usage. We also evaluate the effects of the sampling techniques. Our work and the related evaluation[19, 20] form a complementary study on the efficiency issue of GNNs.

Libraries/Systems for GNNs. PyG [14] and DGL [15] both adopt the message-passing framework as the underlying programming model for GNNs and support training big datasets with the sampling techniques. PyG [14] is built upon PyTorch and it uses optimized CUDA kernels for GNNs to achieve high performance. DGL [15] provides a group of high-level user APIs and supports training GNNs with a variety of backends (TensorFlow, MXNet, and PyTorch) transparently. It also supports LSTM as the aggregation functions. NeuGraph [16] proposes a new programming model *SAGA-NN* for GNNs. It focuses on training big datasets efficiently without sampling. It partitions the dataset sophisticatedly, schedules the training tasks among multiple GPUs, and swaps the data among GPUs and the host asynchronously. AliGraph [17] targets at training GNNs on big attributed heterogeneous graphs that are common in e-commerce platforms. The graphs are partitioned among multiple nodes in a cluster and AliGraph trains GNNs on the graphs in a distributed way with system optimizations. PGL [18] is another graph learning framework from Baidu based on the PaddlePaddle platform.

7. Conclusion and Future Work

In this work, we systematically explore the performance bottlenecks in graph neural network training and inference. We model the existing GNNs with the message-passing framework. We classify the GNNs according to their edge and vertex calculation complexity to select four typical GNNs for evaluation. The experimental results validate our complexity analysis. Fixing other hyper-parameters, the training time, inference time, and memory usage increase linearly with each hyper-parameter of the four GNNs. To find out the performance bottlenecks in the training/inference time, we decompose the training/inference time per epoch on different levels. The time breakdown analysis indicates that the edge calculation stage and its related basic operators are the performance bottlenecks for most GNNs. Moreover, the intermediate results produced by the edge calculation stage cause high memory usage, limiting the data scalability. Adopting sampling techniques can reduce the memory usage of training and inference significantly, without sacrificing accuracy. However, the current implementation of the sampling techniques in PyG brings considerable sampling overheads. The small sampled subgraphs cannot make full use of the computing power of a GPU card either. Our analysis indicates that the edge calculation stage should be the main target of optimizations. Reducing its memory usage and improving its efficiency can significantly improve the performance of GNN training and inference. Based on the analysis, we propose several potential optimizations for the GNN libraries/systems. We believe that our analysis can help developers to have a better understanding of the characteristics of GNN training and inference.

Future Work. Specifically, in this work, we mainly analyze performance bottlenecks of GNN training/inference in the single-GPU environment on static graphs with the message-passing framework. In fact, performance bottlenecks of GNN training/inference over the multi-GPU or distributed environment, dynamic graphs, and other GNN frameworks are also worth studying. In the future, we plan to explore the GNN training/inference performance analysis under the following scenarios:

1. *Multi-GPU or distributed GNN training/inference.* To handle large-scale graph datasets, training/inferring GNNs with the multi-GPU environment or the distributed environment is essential. Multi-GPU and distributed GNN training/inference will inevitably introduce overheads such as inter-GPU and inter-machine communication. How these overheads affect performance bottlenecks is worthy to study.

2. *Spatial-temporal graph datasets.* Spatial-temporal graphs usually have dynamic topology structures. They appear in a variety of applications like traffic speed forecasting [41] and human action recognition [42]. Many new GNNs are proposed to handle this kind of dynamic graphs. The differences of performance issues between these GNNs and the classic GNNs are also worthy of in-depth investigation.

3. *Emerging GNN frameworks.* In this work, we analyzed the widely-used message-passing framework in GNN learning systems. However, some emerging GNN learning systems adopt different frameworks like the SAGA framework [16]. It is interesting to research whether different frameworks would lead to different performance bottlenecks.

Acknowledgements

References

[1] T. N. Kipf, M. Welling, Semi-supervised classification with graph convolutional networks, in: Proceedings of the 5th International Conference on Learning Representations, 2017.
URL https://openreview.net/forum?id=SJU4ayYgl

[2] M. Defferrard, X. Bresson, P. Vandergheynst, Convolutional neural networks on graphs with fast localized spectral filtering, in: Advances in Neural Information Processing Systems, Vol. 29, Curran Associates, Inc., 2016.
URL https://proceedings.neurips.cc/paper/2016/hash/04df4d434d481c5bb723be1b6df1ee65-Abstract.html

[3] R. Li, S. Wang, F. Zhu, J. Huang, Adaptive graph convolutional neural networks, in: Proceedings of the 32nd AAAI Conference on Artificial Intelligence, AAAI, 2018, pp. 3546–3553.
URL https://www.aaai.org/ocs/index.php/AAAI/AAAI18/paper/view/16642

[4] Y. Li, D. Tarlow, M. Brockschmidt, R. S. Zemel, Gated graph sequence neural networks, in: Proceedings of the 4th International Conference on Learning Representations, ICLR, 2016.
URL http://arxiv.org/abs/1511.05493

[5] W. L. Hamilton, Z. Ying, J. Leskovec, Inductive representation learning on large graphs, in: Advances in Neural Information Processing Systems, Vol. 30, Curran Associates, Inc., 2017.
URL https://proceedings.neurips.cc/paper/2017/hash/5dd9db5e033da9c6fb5ba83c7a7ebea9-Abstract.html

[6] P. Velickovic, G. Cucurull, A. Casanova, A. Romero, P. Liò, Y. Bengio, Graph attention networks, in: Proceedings of the 6th International Conference on Learning Representations, 2018.
URL https://openreview.net/forum?id=rJXMpikCZ

[7] J. Zhang, X. Shi, J. Xie, H. Ma, I. King, D. Yeung, Gaan: Gated attention networks for learning on large and spatiotemporal graphs, in: Proceedings of the 34th Conference on Uncertainty in Artificial Intelligence, AUAI Press, 2018, pp. 339–349.
URL http://auai.org/uai2018/proceedings/papers/139.pdf

[8] J. Zhou, G. Cui, Z. Zhang, C. Yang, Z. Liu, L. Wang, C. Li, M. Sun, Graph neural networks: A review of methods and applications, https://arxiv.org/abs/1812.08434 (2018).

[9] Z. Zhang, P. Cui, W. Zhu, Deep learning on graphs: A survey, IEEE Transactions on Knowledge and Data Engineering (Early Access) (2020) 1–1. doi:10.1109/TKDE.2020.2981333.

[10] Z. Wu, S. Pan, F. Chen, G. Long, C. Zhang, P. S. Yu, A comprehensive survey on graph neural networks, IEEE Transactions on Neural Networks and Learning Systems 32 (1) (2021) 4–24. doi:10.1109/TNNLS.2020.2978386.

[11] S. Qi, W. Wang, B. Jia, J. Shen, S. Zhu, Learning human-object interactions by graph parsing neural networks, in: V. Ferrari, M. Hebert, C. Sminchisescu, Y. Weiss (Eds.), Proceedings of the European Conference on Computer Vision (ECCV), Vol. 11213 of Lecture Notes in Computer Science, Springer, 2018, pp. 407–423. doi:10.1007/978-3-030-01240-3_25.

[12] W. Wang, H. Zhu, J. Dai, Y. Pang, J. Shen, L. Shao, Hierarchical human parsing with typed part-relation reasoning, in: Proceedings of the 2020 IEEE/CVF Conference on Computer Vision and Pattern Recognition, IEEE, 2020, pp. 8926–8936. doi:10.1109/CVPR42600.2020.00895.

[13] W. Wang, X. Lu, J. Shen, D. J. Crandall, L. Shao, Zero-shot video object segmentation via attentive graph neural networks, in: Proceedings of the 2019 IEEE/CVF International Conference on Computer Vision, IEEE, 2019, pp. 9235–9244. doi:10.1109/ICCV.2019.00933.

[14] M. Fey, J. E. Lenssen, Fast graph representation learning with pytorch geometric, https://arxiv.org/abs/1903.02428 (2019).

[15] M. Wang, L. Yu, D. Zheng, Q. Gan, Y. Gai, Z. Ye, M. Li, J. Zhou, Q. Huang, C. Ma, Z. Huang, Q. Guo, H. Zhang, H. Lin, J. Zhao, J. Li, A. J. Smola, Z. Zhang, Deep graph library: Towards efficient and scalable deep learning on graphs, https://arxiv.org/abs/1909.01315v1 (2019).

[16] L. Ma, Z. Yang, Y. Miao, J. Xue, M. Wu, L. Zhou, Y. Dai, Neugraph: Parallel deep neural network computation on large graphs, in: Proceedings of the 2019 USENIX Annual Technical Conference, USENIX Association, 2019, pp. 443–458.
URL https://www.usenix.org/conference/atc19/presentation/ma

[17] R. Zhu, K. Zhao, H. Yang, W. Lin, C. Zhou, B. Ai, Y. Li, J. Zhou, Aligraph: A comprehensive graph neural network platform, Proceedings of the VLDB Endowment 12 (12) (2019) 2094–2105. doi:10.14778/3352063.3352127.

[18] Baidu, Paddle graph learning, https://github.com/PaddlePaddle/PGL.

[19] M. Yan, Z. Chen, L. Deng, X. Ye, Z. Zhang, D. Fan, Y. Xie, Characterizing and understanding GCNs on GPU, IEEE Computer Architecture Letters 19 (1) (2020) 22–25. doi:10.1109/LCA.2020.2970395.

[20] Z. Zhang, J. Leng, L. Ma, Y. Miao, C. Li, M. Guo, Architectural implications of graph neural networks, IEEE Computer Architecture Letters 19 (1) (2020) 59–62. doi:10.1109/LCA.2020.2988991.

[21] B. Perozzi, R. Al-Rfou, S. Skiena, Deepwalk: online learning of social representations, in: Proceedings of the 20th ACM SIGKDD International Conference on Knowledge Discovery and Data Mining, ACM, 2014, pp. 701–710. doi:10.1145/2623330.2623732.

[22] A. Grover, J. Leskovec, node2vec: Scalable feature learning for networks, in: Proceedings of the 22nd ACM SIGKDD International Conference on Knowledge Discovery and Data Mining, ACM, 2016, pp. 855–864. doi:10.1145/2939672.2939754.

[23] J. Gilmer, S. S. Schoenholz, P. F. Riley, O. Vinyals, G. E. Dahl, Neural message passing for quantum chemistry, in: Proceedings of the 34th International Conference on Machine Learning, Vol. 70, PMLR, 2017, pp. 1263–1272.
URL http://proceedings.mlr.press/v70/gilmer17a.html

[24] D. K. Duvenaud, D. Maclaurin, J. Iparraguirre, R. Bombarell, T. Hirzel, A. Aspuru-Guzik, R. P. Adams, Convolutional networks on graphs for learning molecular fingerprints, in: Advances in Neural Information Processing Systems, Vol. 28, Curran Associates, Inc., 2015.
URL https://proceedings.neurips.cc/paper/2015/hash/f9be311e65d81a9ad8150a60844bb94c-Abstract.html

[25] H. Dai, Z. Kozareva, B. Dai, A. J. Smola, L. Song, Learning steady-states of iterative algorithms over graphs, in: Proceedings of the 35th International Conference on Machine Learning, Vol. 80, PMLR, 2018, pp. 1114–1122.
URL http://proceedings.mlr.press/v80/dai18a.html

[26] W.-L. Chiang, X. Liu, S. Si, Y. Li, S. Bengio, C.-J. Hsieh, Cluster-GCN: An efficient algorithm for training deep and large graph convolutional networks, in: Proceedings of the 25th ACM SIGKDD International Conference on Knowledge Discovery and Data Mining, ACM, 2019, pp. 257–266. doi:10.1145/3292500.3330925.

[27] R. Ying, R. He, K. Chen, P. Eksombatchai, W. L. Hamilton, J. Leskovec, Graph convolutional neural networks for web-scale recommender systems, in: Proceedings of the 24th ACM SIGKDD International Conference on Knowledge Discovery and Data Mining, ACM, 2018, pp. 974–983. doi:10.1145/3219819.3219890.

[28] J. Chen, T. Ma, C. Xiao, FastGCN: Fast learning with graph convolutional networks via importance sampling, in: Preceedings of the 6th International Conference on Learning Representations, 2018.
URL https://openreview.net/forum?id=rytstxWAW

[29] J. Chen, J. Zhu, L. Song, Stochastic training of graph convolutional networks with variance reduction, in: Proceedings of the 35th International Conference on Machine Learning, Vol. 80, PMLR, 2018, pp. 942–950.
URL http://proceedings.mlr.press/v80/chen18p.html

[30] H. Zeng, H. Zhou, A. Srivastava, R. Kannan, V. K. Prasanna, Accurate, efficient and scalable graph embedding, in: Proceedings of the 2019 IEEE International Parallel and Distributed Processing Symposium, IEEE, 2019, pp. 462–471. doi:10.1109/IPDPS.2019.00056.

[31] H. Zeng, H. Zhou, A. Srivastava, R. Kannan, V. K. Prasanna, Graphsaint: Graph sampling based inductive learning method, in: Proceedings of the 8th International Conference on Learning Representations, 2020.
URL https://openreview.net/forum?id=BJe8pkHFwS

[32] W. Huang, T. Zhang, Y. Rong, J. Huang, Adaptive sampling towards fast graph representation learning, in: Advances in Neural Information Processing Systems, Vol. 31, Curran Associates, Inc., 2018.
URL https://proceedings.neurips.cc/paper/2018/hash/01eee509ee2f68dc6014898c309e86bf-Abstract.html

[33] O. Shchur, M. Mumme, A. Bojchevski, S. Günnemann, Pitfalls of graph neural network evaluation, http://arxiv.org/abs/1811.05868 (2018).

[34] J. Yang, J. Leskovec, Defining and evaluating network communities based on ground-truth, in: Proceedings of the 12th IEEE International Conference on Data Mining, IEEE, 2012, pp. 745–754. doi:10.1109/ICDM.2012.138.

[35] D. Chakrabarti, Y. Zhan, C. Faloutsos, R-mat: A recursive model for graph mining, Proceedings of the 2004 SIAM International Conference on Data Mining, pp. 442–446. doi:10.1137/1.9781611972740.43.

[36] D. P. Kingma, J. Ba, Adam: A method for stochastic optimization, in: Proceedings of the 3rd International Conference on Learning Representations, 2015.
URL http://arxiv.org/abs/1412.6980

[37] X. Glorot, Y. Bengio, Understanding the difficulty of training deep feedforward neural networks, in: Proceedings of the Thirteenth International Conference on Artificial Intelligence and Statistics, Vol. 9, JMLR Workshop and Conference Proceedings, 2010, pp. 249–256.
URL http://proceedings.mlr.press/v9/glorot10a.html

[38] T. Chen, B. Xu, C. Zhang, C. Guestrin, Training deep nets with sublinear memory cost, https://arxiv.org/abs/1604.06174 (2016).

[39] V. P. Dwivedi, C. K. Joshi, T. Laurent, Y. Bengio, X. Bresson, Benchmarking graph neural networks, https://arxiv.org/abs/2003.00982 (2020).

[40] W. Hu, M. Fey, M. Zitnik, Y. Dong, H. Ren, B. Liu, M. Catasta, J. Leskovec, Open graph benchmark: Datasets for machine learning on graphs, in: Advances in Neural Information Processing Systems, Vol. 33, Curran Associates, Inc., 2020.
URL https://proceedings.neurips.cc/paper/2020/hash/fb60d411a5c5b72b2e7d3527cfc84fd0-Abstract.html

[41] Y. Li, R. Yu, C. Shahabi, Y. Liu, Diffusion convolutional recurrent neural network: Data-driven traffic forecasting, in: Proceedings of the 6th International Conference on Learning Representations, 2018.
URL https://openreview.net/forum?id=SJiHXGWAZ

[42] S. Yan, Y. Xiong, D. Lin, Spatial temporal graph convolutional networks for skeleton-based action recognition, in: Proceedings of the 32nd AAAI Conference on Artificial Intelligence, AAAI, 2018, pp. 7444–7452.
URL https://www.aaai.org/ocs/index.php/AAAI/AAAI18/paper/view/17135